Composite Structures 331 (2024) 117901

Contents lists available at ScienceDirect

Composite Structures

journal homepage: www.elsevier.com/locate/compstruct

A novel design model for predicting the shear resistance of reinforced concrete beams strengthened with EBR-CFRP systems

Amirhossein Mohammadi *, Joaquim A.O. Barros, José Sena-Cruz

University of Minho, ISISE, ARISE, IB-S, Department of Civil Engineering, 4800-058 Guimarães, Portugal

ARTICLE INFO

Keywords:
Design model
Shear strengthening
Reinforced concrete beams
Externally bonded reinforcements
FRP
Reliability analysis

ABSTRACT

Shear resistance prediction of reinforced concrete (RC) beams strengthened with externally bonded reinforcements (EBR) is a challenging task due to the complex nature of shear resisting mechanisms and their intricate interaction. Existing design models often overlook these dependencies, leading to significant variations in prediction accuracy. In this paper, a design model is proposed by integrating the most relevant shear resisting mechanisms based on the evidence demonstrated by a large database of experimental results from RC beams shear strengthened with wet layup carbon fibre reinforced (CFRP) sheets applied according to the EBR technique. The developed approach integrates the simplified modified compression field theory (SMCFT) with a regression-based model. A global sensitivity analysis was conducted according to which closed form equations were derived to obtain the tensile stress factor in cracked concrete and the inclination angle of the critical diagonal crack. A reliability analysis is carried out, and resistance reduction factors are achieved for different levels of reliability index. The database, composed of 284 RC beams shear strengthened with EBR-CFRP technique, is utilized to validate the proposed model, and compare its performance against some well-established existing design models. The results show that the proposed model, with an adequate framework for its use on design practice, outperforms the other considered models.

1. Introduction

Carbon fibre reinforced polymer (CFRP) reinforcements applied according to the externally bonded reinforcement (EBR) have been demonstrated to be very efficient for increasing the shear capacity of reinforced concrete (RC) [1,2], being the unique technique with a design-based formulation in the *fib* bulletin 90 [3]. The literature offers various models for predicting the increase in shear resistance of RC beams strengthened with EBR-FRP systems. These models can be categorized into two main approaches. A semi-empirical type approach, where the governing variables, typically the effective strain or stress of the FRP system, are determined through curve fitting of experimental data [4,5] or by applying optimization algorithms using available data [6]. The second type of approach is mechanic-based, aiming to simulate the shear resisting mechanics [7,8]. The former approach is relatively simple to develop and easy to apply in design practice, but its predictive performance highly depends on the quality and relevance of the database. The mechanics-based type-approaches require more complex calculations, but have the potential of providing more reliable results. Some ambiguity on how to consider the contribution of concrete, existing steel reinforcements and FRP for the shear resistance of a RC beam, and the use of partially safety factors for the materials or the global safety factor for the model introduces extra difficulties for the designer [6–9]. Design codes and guidelines have recommended some equations for predicting the design value of shear resistance in RC beams shear strengthened with EBR-FRP systems; however, recent studies have shown their debilities in terms of predicting the shear resistance with required accuracy and reliability [10,11]. Therefore, there is a need to develop more accurate and reliable design models.

Mohammadi *et al.* [10] proposed a model for predicting the contribution of CFRP to the shear resistance of RC beams strengthened with EBR-FRP reinforcements. Their model demonstrated some improvement in predicting the contribution of CFRP reinforcement over other selected existing models. This was assured by considering in the formulation the influence of various factors, such as the interaction between existing steel stirrups and FRP reinforcement, the shear strengthening configuration, and the radius of the corners in beam cross-section. In the present paper, the model of Mohammadi *et al.* [10] is improved by considering

* Corresponding author.
E-mail addresses: id9251@alunos.uminho.pt (A. Mohammadi), barros@civil.uminho.pt (J.A.O. Barros), jsena@civil.uminho.pt (J. Sena-Cruz).

https://doi.org/10.1016/j.compstruct.2024.117901
Received 13 October 2023; Received in revised form 11 December 2023; Accepted 8 January 2024
Available online 10 January 2024

the influence of the ratio of longitudinal steel bars. The model then is integrated with the simplified compression field theory (SMCFT) to determine more rigorously the inclination of the critical diagonal crack (CDC), θ, and the tensile stress factor (ζ) that accounts the contribution of the cracked concrete for the shear resistance of RC beams shear strengthened with EBR-CFRP systems [12]. The application of SMCFT equations involves, however, an iterative process, posing additional challenges from a design standpoint [13]. To avoid this iterative process, a global sensitivity analysis is conducted to identify the key parameters influencing ζ and θ. The relation between these key parameters and ζ is established using a hyperplane fitting technique. Additionally, a strong correlation is observed between ζ and θ, enabling the estimation of θ through a curve fitting process that captures the relationship between these variables.

It has been verified that the web of T cross section type beams contributes significantly to their shear capacity [14–16]. In RC beams shear strengthened with EBR-CFRP systems this contribution can reach up to 45 % of the total beam's shear strength [17]. Therefore, the influence of the flange in beams with T-shaped cross-section on shear capacity of RC beams failing in shear is considered in the proposed model.

To ensure the practical applicability of the proposed closed-form model in design scenarios, a reliability analysis is conducted [18–20]. This analysis involves determining various resistance reduction factors corresponding to different levels of reliability indices. To validate the model, a reliable dataset composed of 284 experimental results of beams shear strengthened with the EBR technique is taken from a larger database called DABASUM [21]. This dataset served as the basis for evaluating the predictive performance of the proposed model, as well as comparing it with other well-known design models, namely: *fib* bulletin 90 (*fib* TG5.1) [3], ACI440-2R-17 [22] and TR55 [23]. The selected models are widely used by professionals and researchers in the field. A comprehensive introduction to the formulations of these models is given in Appendix A.

2. Proposed model (MBS)

In this section, a novel model for predicting the shear resistance of RC beams shear strengthened with EBR-CFRP sheets is described. This model, abbreviated by MBS, combines the SMCFT with the improved formulation of model proposed by Mohammadi *et al.* (2023) [10]. The shear resistance is evaluated using the following equation (the physical meaning of the adopted symbols is illustrated in Fig. 1):

$$V_{Rd}^{\mathrm{MBS}} = \phi \nu b_w d_s \tag{1a}$$

$$\nu = \nu_c + \nu_s + \nu_f \tag{1b}$$

where ϕ is a resistance reduction factor, whose value will be determined by reliability analysis in section 4, b_w (in mm) is the width of the beam's web, d_s (in mm) is the depth of the beam's tensile reinforcement, ν is shear strength; ν_c, ν_s, and ν_f represent the respective contribution of concrete, steel, and FRP that can be determined from the following equations:

$$\nu_c = k_f \zeta \sqrt{f_{cm}} \tag{2}$$

$$\nu_s = \rho_{sw} f_{swy} \cot\theta \tag{3}$$

$$\nu_f = \frac{V_f}{b_w d} = \frac{A_{fwc} h_f E_f \varepsilon_{fe}}{b_w d_s} \left(\cot\theta + \cot\alpha_f\right) \sin\alpha_f \tag{4}$$

In Eqs. (2) and (3), f_{cm} (in MPa) is the concrete average compressive strength, k_f is a shape factor accounting for the extra shear fracture surface at the web-flange connection occurred in T-shaped section, proposed by RILEM TC162-TDF [24], and determined from Eq. (6), ζ is a factor to take into account that concrete is cracked in the shear failure region (also known as tensile stress factor), obtained from Eq. (7) [12], ρ_{sw} and f_{swy} (in MPa) are the ratio and the yield stress of existing transverse steel reinforcement. In Eq. (4) A_{fwc} is the effective CFRP cross-section area calculated as $2w_f t_f / s_f$ for strips and $2t_f \sin\alpha_f$ for continuous CFRP sheets, being w_f, t_f and s_f the width, the thickness and the spacing of CFRP strips (in mm); α_f is the angle between the longitudinal axis of the beam and the fibres of these strips, as depicted in Fig. 1. ε_{fe} is the effective strain in the CFRP, obtained from Mohammadi et al.'s model [10]. To enhance the prediction performance of this model, adjustments were made to its coefficients, and another important variable, the ratio of longitudinal bars in tension (ρ_l) was incorporated into the model. The ratio of longitudinal bars in tension are found to change the strain distribution at CFRP reinforcement along the CDC, consequently influencing ε_{fe}. These modifications led to a 10 % decrease in coefficient of variation (*CoV*) of the model uncertainty.

The modified prediction model for obtaining ε_{fe} is as follow:

$$\varepsilon_{fe} = m_F \times \left(1 - 0.0011 E_f \rho_f / f_{cm}^{2/3}\right) \times \left(E_f \rho_f / f_{cm}^{2/3}\right)^{-0.62}$$

with,

$$m_F = 0.013 \times \kappa_{sw} \kappa_R \kappa_{O/U} \kappa_{sl};$$

$$\kappa_{sw} = 1 - 25.4\rho_{sw}; \kappa_R = 0.75\left(\frac{R_c}{50}\right) + 0.7 \leqslant 1.45; \kappa_{O/U} = 1 + 0.52\kappa; \kappa_{sl} = 1 + 12.5\rho_l \tag{5}$$

where E_f and ρ_f are the elastic modulus and ratio of CFRP reinforcement; R_c is the corner radius of beam's cross section; κ is the strengthening configuration factor, being 1.0 for fully wrapped and 0 for U-wrapped beams, respectively.

$$k_f = 1 + n\frac{h_{fl}^2}{b_w d_s} \leqslant 1.5 n = \frac{b_{fl} - b_w}{h_{fl}} \leqslant 3 \tag{6}$$

where b_{fl} and h_{fl} are the width and thickness of the beam flange.

$$\zeta = \frac{0.4}{1 + 1500\varepsilon_x} \frac{1300}{1000 + s_{xe}} \tag{7}$$

where s_{xe} is the crack spacing:

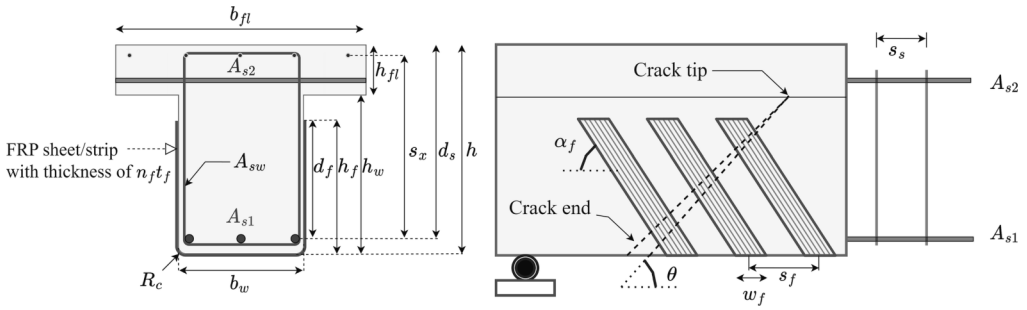

Fig. 1. The Symbols of geometric properties entities of a RC beam shear strengthened with of externally bonded CFRP on the strengthened RC beam.

$$s_{xe} = \frac{35 s_x}{a_g + 16} \geqslant 0.85 s_x \tag{8}$$

being s_x (in mm) the vertical distance between longitudinal bars; a_g (in mm) is the maximum aggregate size, and ε_x is the longitudinal strain at mid depth of the beam's cross section ($h/2$):

$$\varepsilon_x = \min\left(\frac{\nu \cot\theta - \nu_c/\cot\theta}{E_{sl}\rho_{sl}}, \varepsilon_{sy}\right) \tag{9}$$

where E_{sl} and ρ_{sl} are the modulus of elasticity and ratio of longitudinal reinforcements (tensile and compressive steel rebars, i.e.,$\rho_{sl} = (A_{s1} + A_{s2})/b_w d_s$) and ε_{sy} is its yield strain.

θ in Eqs. (3), (4), and (9) is inclination angle, in degrees, of the CDC in the web of the section, determined from [12]:

$$\theta = (29 + 7000\varepsilon_x)\left(0.88 + \frac{s_{xe}}{2500}\right) \leqslant 75^\circ \tag{10}$$

Fig. 2 presents the steps of the iterative procedure to calculate the shear strength of a RC beam according to MBS model.

3. Sensitivity analysis

The initial formulation of MBS model requires an iterative procedure to determine the shear capacity of the beam. To avoid the inconveniences of an iterative procedure in design practice, a strategy is adopted for obtaining ζ and θ, with minimum loss of accuracy, by employing a global sensitivity analysis [13]. Unlike local sensitivity analysis, global sensitivity analysis evaluates the output by simultaneously varying all input parameters [25]. This sensitivity analysis allows the assessment of the dependence of the model's output on the selected values of the input parameters. To perform the analysis, a random selection of input variables needs to be made, followed by the evaluation of the corresponding outputs (i.e., θ, ζ and ν) using the procedure outlined in Fig. 2. A sample set of 5000 beams was generated using a Latin Hypercube Sampling (LHS) method considering a uniform distribution of input variables (Δ), ensuring an equal probability of occurrence for each value within the adopted range for the considered variables, as shown in Table 1. This process results in the generation of a comprehensive dataset consisting of input–output pairs, which can be further analysed and investigated.

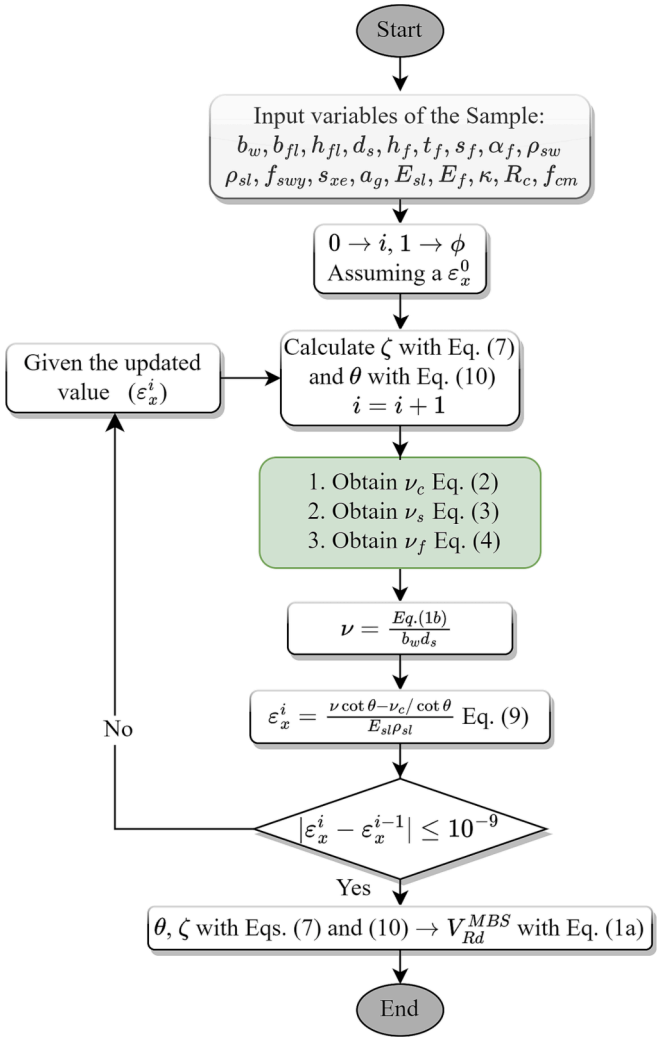

Fig. 2. Calculation procedure of MBS model.

To assess the significance of each parameter on the outputs, a dimensionless parameter, denoted as σ, was employed. This parameter is obtained from the following equation [13]:

$$\sigma_{ij} = \frac{n\sum_{k=1}^{n} I_{ik} O_{jk} - \left(\sum_{k=1}^{n} O_{jk}\right)\left(\sum_{k=1}^{n} I_{ik}\right)}{\sqrt{n\left(\sum_{k=1}^{n} I_{ik}^2\right) - \left(\sum_{k=1}^{n} I_{ik}\right)^2}\sqrt{n\left(\sum_{k=1}^{n} O_{jk}^2\right) - \left(\sum_{k=1}^{n} O_{jk}\right)^2}} \tag{11}$$

where n is the number of samples ($n = 5000$); I_i is the i^{th} input parameter (e.g., f_{cm}); and O_j is the j^{th} output parameters (e.g., θ). The σ parameter can range from -1 to $+1$, with positive and negative signs indicating positive and negative linear correlations, respectively. A positive value of σ suggests that as the independent variable I_i increases, the dependent variable O_j also increases, and vice versa. Conversely, a negative value of σ indicates that O_j decreases with the increase of I_i, and O_j increases with the decrease of I_i. When the σ value is close to 0, signifies either a weak linear correlation or no linear correlation between the variables. The values of the σ for each input parameter and output entity is given in Fig. 3.

As can be seen, the ρ_{sw}, f_{swy}, ρ_{sl} and h_f exhibit the highest influence on the outputs. The b_w and b_{fl} also have significance, but they were intentionally omitted from consideration to avoid the potential multicollinearity issue and complexity of equations without improvement in the prediction accuracy. These selected parameters play a crucial role in a model for predicting ζ and θ. It is noteworthy that a strong correlation between ζ and θ is expected [13]. Consequently, by initially predicting one of these parameters and subsequently calculating the other one based on this predicted parameter, the iterative procedure of the model can be eliminated. In the following, an equation will be introduced to approximate the value of ζ found from Eq. (7), thereby facilitating the subsequent calculation of θ. Fig. 4 shows that there is a strong relation between ζ and the following composite parameters $x = \rho_{sw} f_{swy}$, $y = \rho_{sl}$,

Table 1
Design space of input variables (meaning of the symbols in Fig. 1).

Random variable	Range
Web width,b_w	[75 −600] mm with Δb_w = 5 mm
Flange width,b_{fl}	[b_w − 3b_w]mm with $\Delta b_{fl} = 0.5 b_w$
Flange thickness,h_{fl}	{0, 50, 100} mm
Height of beam's cross section,h	[b_w − 2b_w] mm with Δh = 5 mm
Corner radius,R_c	{10, 20, 30, 40} mm
Fibre's angle,α_f	{45, 60, 75, 90} degrees
Young modulus of elasticity of FRP,E_f	[60 −400] GPa with ΔE_f = 20 GPa
FRP strengthening ratio,ρ_f	[0.8 − 20]‰
Flexural reinforcement ratio of steel bars, ρ_{sl}	[1 − 7.5]%
Transverse reinforcement ratio of steel stirrups, ρ_{sw}	[0 − 1.8]%
Yield stress of steel stirrups, f_{swy}	[240 −670] MPa with Δf_{swyk} = 10 MPa
Mean concrete compressive strength,f_{cm}	[20 − 100] MPa with Δf_{cm} = 1 MPa
Maximum dimension of aggregates,a_g	[10 − 40]mm with Δa_g = 1 mm

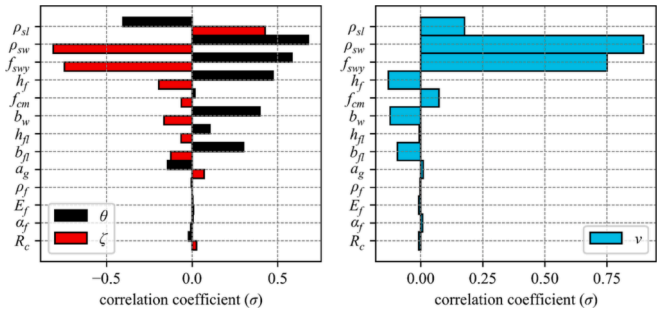

Fig. 3. Tornado plots; calculated via sensitivity analysis for MBS model.

and $w = h_f$. To find the relationship between ζ and these parameters a hyperplane should be fitted to the data. A hyperplane, described by the following form, is determined to be the best fit for the available data:

$$\zeta_{MBC} = \left(ax_i^b + cy_i^d\right) \times \left(w_i^e + f\right) \tag{12}$$

where ζ_{MBS} represents the fitted hyperplane to ζ (found by Eq. (7)) and a, b, c, d, e and f are the unknown constants of this hyperplane. To derive this hyperplane and to obtain the corresponding constants, an objective function is defined, and genetic algorithm was employed:

$$L = \sum_{i=1}^{n} \left| \frac{\zeta_i - \zeta_{MBC,i}}{\zeta_i} \right| \tag{13}$$

By minimizing the objective function, the constants are determined and the best fit of the hyperplane to the data is represented as follow:

$$\zeta_{MBS} = \left(0.49y^{0.19} - 0.066x^{0.37}\right)(1.11 - 0.00021w)$$
$$\text{where } 0.05 < \zeta_{MBS} \leqslant 0.35 \tag{14}$$

Fig. 4a clearly illustrates the interrelation between θ and ζ. Considering this relationship, a power function is fitted to the data, resulting in a prediction model for θ based on the ζ value (Eq. (15)).

$$\theta_{MBS} = 4.06\zeta_{MBS}^{-0.75} + 20.7 \quad 29 < \theta_{MBS} \leqslant 60 \tag{15}$$

The goodness of the fit is shown by the following statistical metrics:

$$RMSE = \sqrt{\sum_{i=1}^{n} (y_i - \gamma_i)^2 \Big/ n} \tag{16}$$

$$MAPE = \frac{100\%}{n} \sum_{i=1}^{n} (|(y_i - \gamma_i)/y_i|) \tag{17}$$

$$R^2 = 1 - \left(\sum_{i=1}^{n} (y_i - \gamma_i)^2 \Big/ \sum_{i=1}^{n} (y_i - \bar{y})^2 \right) \tag{18}$$

$$r = \sum_{i=1}^{n} \left[\frac{(\gamma_i - \bar{\gamma})(y_i - \bar{y})}{\sqrt{\sum_{i=1}^{n} (\gamma_i - \bar{\gamma})^2 \sum_{i=1}^{n} (y_i - \bar{y})^2}} \right] \tag{19}$$

where *RMSE* is the root mean square error; *MAPE* is the mean absolute percentile error; R^2 is the coefficient of determination; r is the Pearson correlation coefficient; y_i (i.e., ζ and θ obtained from MBS-SMCFT) is the actual value for the i^{th} sample; $\bar{y}$ is the mean of actual values; γ_i (i.e., ζ_{MBS} and θ_{MBS} obtained from approximate solution) is the predicted value for the i^{th} sample, and $\bar{\gamma}$ is the mean value of predicted values. A model with a perfect prediction has a null value for *MAPE* and *RMSE* and the unitary value for r and R^2. The *RMSE*, *MAPE*, R^2 and r for the fitted hyperplane (ζ_{MBS}) for ζ are 0.013, 4.60 %, 0.96, and 0.98, respectively. As the fitted hyperplane cannot be easily visualized in a three-dimensional plot, two fixed values of w were chosen, and two different planes are plotted in Fig. 4b, corresponding to these values. The accuracy of the fitted curve (θ_{MBS}) for θ was assessed using introduced statistical metrics. The *RMSE*, *MAPE*, R^2 and r were 1.71, 3.51 %, 0.86, and 0.93, respectively.

4. Resistance reduction factor

In design applications, it is common to use a reduced value of resistance, commonly considered the design value of the resistance (R_d). This reduced value can be obtained by applying a resistance reduction factor (ϕ). The objective in this section is to calibrate strength reduction factors for the MBS model, taking into account uncertainties and variations, to ensure structural safety and to achieve desired target reliability indices (β_T). The choice of the target reliability index (β_T) in the context of the ultimate limit state is generally influenced by various factors, including the consequences of failure, relative costs of safety measures, and the reference period, as discussed in [26]. According to [26], the selection of the target reliability index for existing structures depends on the costs associated with implementing safety measures. It is recommended to consider a target reliability index within the range of 3.1 to 4.1, with different values corresponding to different cost considerations and specified reference periods. In this study, four levels of target reliability are considered to capture a range of safety and cost scenarios. The selected target reliability indices are $\beta_T = 3.1$, $\beta_T = 3.4$, $\beta_T = 3.8$ and $\beta_T = 4.1$. In the case of new elements a β_T of 3.8 is recommended [26], which is adopted in this study to compare the proposed model with other considered models. Monte Carlo Simulation (MCS) is a comprehensive and rigorous approach to determine the probability of failure and consequently ϕ values [18,27], which is also employed in

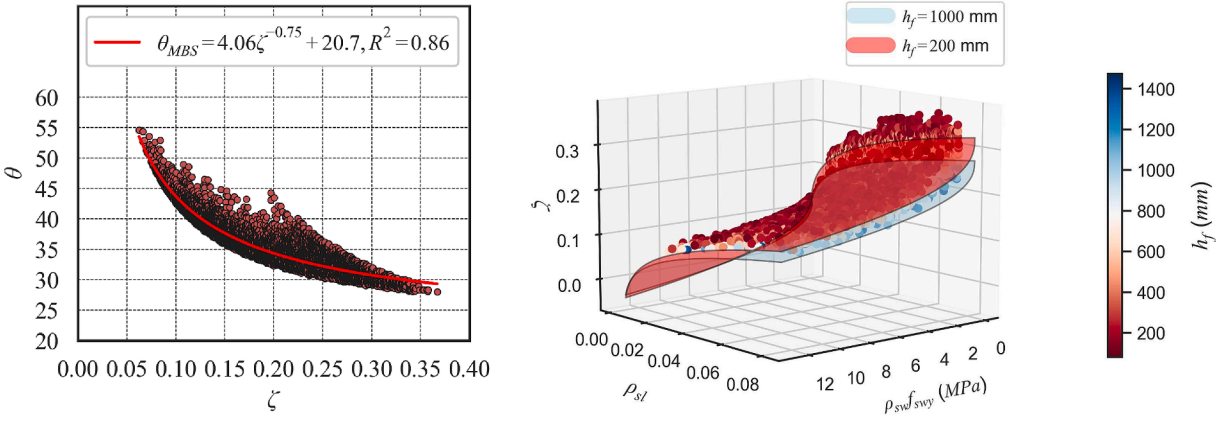

Fig. 4. A) interrelation between θ and ζ; b) ζ values obtained from MBS model and the planes fitting the data with two different h_f.

this study. The MCS is known for its accuracy in capturing the uncertainties and variability associated with the structural behaviour, material properties, etc. Although this approach can be computationally intensive and time-consuming.

Fig. 5 presents the flowchart of the reliability analysis performed in this paper using MCS method. In this analysis four different ϕ values are to determine considering the selected target reliability indices. The analysis initiates by generating 100 beam samples using LHS within specified parameter ranges as outlined in Fig. 5. The properties of each beam sample required for MBS model are subsequently stored in a vector denoted as $\vec{x}_m$, comprising p parameters. Then, for each value of ϕ (ranging from 0.1 to 1, with an increments of 0.01), a reliability index is obtained for all the samples adopting five different values of live load to dead load ratio ($\alpha = Q_{LL}/Q_{DL}$), as recommended in [18,20] (i.e., 0.5,1.0,1.5,2.0, and 2.5). It should be noted that the selected number of samples are sufficient, as further increasing the sample size does not yield significant difference in the outcome.

The solution procedure to calculate β is presented in a nested flowchart in Fig. 5. Initially, the load distribution (**Q**) is obtained as the sum of the dead and live load distributions ($\boldsymbol{Q}_{DL}$ and $\boldsymbol{Q}_{LL}$) without considering any load factors. The distribution of dead and live load can be obtained by taking the respective nominal values of dead load and live loads (Q_{DL} and Q_{LL}) as mean, and the statistical characteristics of dead and live load given in Table 2. To obtain Q_{DL} and Q_{LL}, an indirect method is used as described in [19,20]. The ultimate limit state load combination (Q_{ULS}), as defined by ACI 318 [28], is considered. This load combination considers the dead load (Q_{DL}) and live load (Q_{LL}) majored according to the following load factors:

$$Q_{ULS} = 1.2Q_{DL} + 1.6Q_{LL} \tag{20}$$

Based on the limit state design function (i.e., $R_d = Q_{ULS}$) and Eq. (20), Respective Q_{DL} and Q_{LL} can be expressed as:

$$Q_{DL} = \frac{R_d}{1.2 + 1.6\,\alpha} \tag{21}$$

$$Q_{LL} = \frac{\alpha R_d}{1.2 + 1.6\,\alpha} \tag{22}$$

The design resistance (R_d) is calculated using Eq. (1a) with the given $\vec{x}_m$ and the corresponding ϕ.

Simultaneously, the distribution of resistance (**R**) is obtained (using Eq. (1a) and ϕ of equal to 1.0) considering the distribution of random variables (**X**) with their respective means in $\vec{x}_m$ and the statistical characteristics in Table 2. The size of samples for MCS is denoted as N and is set to 2,000,000.

To consider the model uncertainty the distribution of model error should be identified. According to the Kolmogorov-Smirnov (K-S) testing model uncertainty $\chi = V_R^{exp}/V_R^{MBS}$ (with V_R^{exp} and V_R^{MBS} being the experimental values in the database introduced in the section 5.1 and the model prediction of the shear resistance, respectively) is identified to have an Extreme type I distribution with a mean of 1.0 and *Cov* of 0.3, as can be seen in Fig. 6.

Hence, a random variable of size N is sampled from this distribution to represent the model error distribution (χ). Having the **R**, **Q**, and χ distribution, the ultimate limit state function (**g**) of the beam sample is adopted to differentiate the acceptable and unacceptable structural state of the beam, which is given as

$$\boldsymbol{g}(\boldsymbol{X}) = \boldsymbol{\chi}\boldsymbol{R}(\boldsymbol{X}) - \boldsymbol{Q}(\boldsymbol{X}) \tag{23}$$

An unacceptable state or often known as failure state can be represented as $\boldsymbol{g}(\boldsymbol{X}) \leqslant 0$. If the random vector of variables is represented by a joint probability density function $\mathrm{X} \sim f(\mathbf{X})$, the failure probability p_f can be computed by

$$p_f = P(g(\boldsymbol{X}) \leqslant 0) = \int_{\{X:g(X)\leqslant 0\}} f(\boldsymbol{X})d\boldsymbol{X} \tag{24}$$

However, when using MCS the functional form of f (**X**) is not available, therefore the expected value of p_f is calculated as the fraction of samples that belong to the failure domain n_f (g(x) ≤ 0) over N.

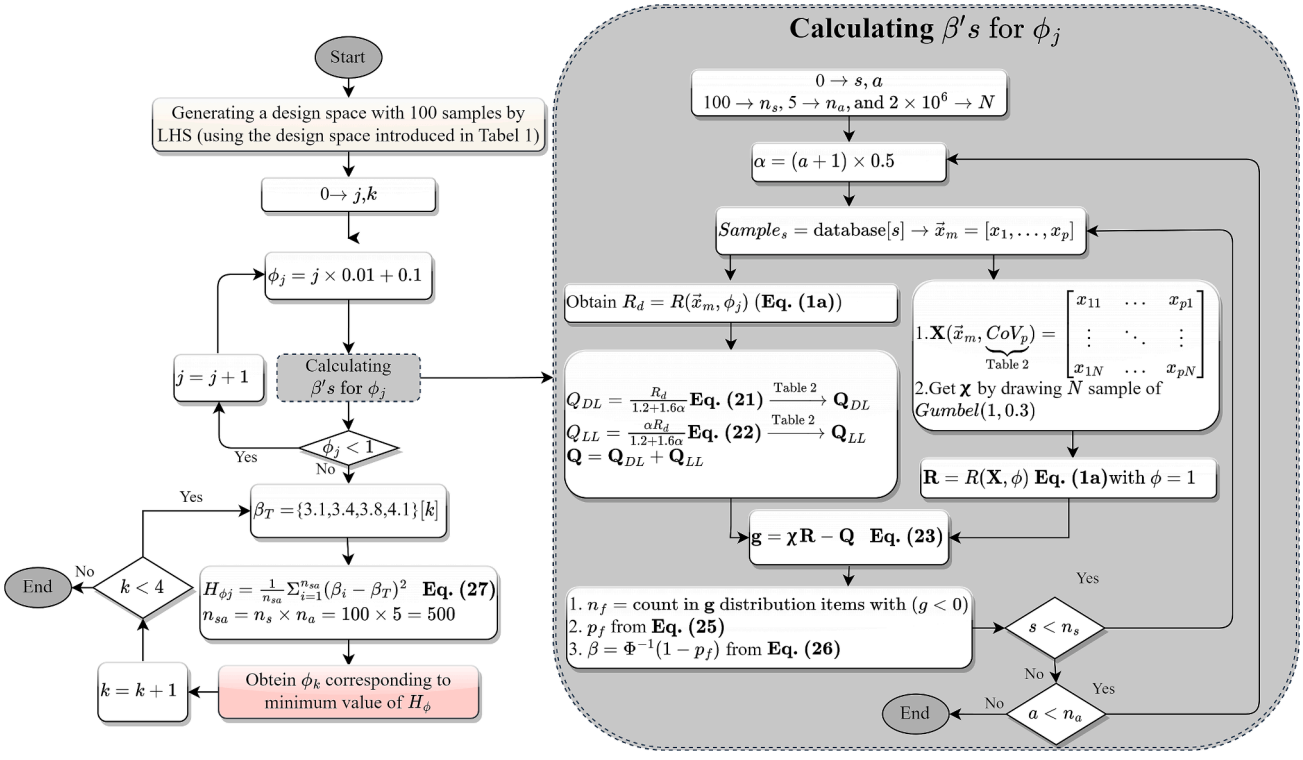

Fig. 5. Reliability index prediction and resistance reduction factor calibration.

Table 2
Statistical characteristics of random variables.

Random variable	Bias [29]	*CoV*	Distribution	Reference
Web width (b_w)	1	0.02	Normal	[30]
Total height (h)	1	0.01	Normal	[30]
Effective depth (d)	1	0.02	Normal	[30]
Corner radius (R_c)	1	0.05	Normal	assumed
Fibre's angle (α_f)	1	0.05	Normal	[31]
Young modulus of CFRP (E_f)	1	0.02	Normal	[20]
Young modulus of steel (E_s)	1	0.024	Normal	[32]
CFRP shear strengthening ratio (ρ_f)	1	0.03	Normal	[19]
Reinforcement ratio of longitudinal steel bars (ρ_{sl})	1	0.05	Normal	assumed
Reinforcement ratio of transversal steel bars (ρ_{sw})	1	0.05	Normal	assumed
Yield stress of steel stirrups (f_{swy})	1.1	0.075	Normal	[33]
Mean concrete compressive strength (f_{cm})	1.15	0.1	Lognormal	[34]
Model Error (χ)	1	0.3	Extreme I	k-s test
Dead load (Q_{DL})	1	0.1	Normal	[34]
Live load (Q_{LL})	1 + 0.14ln(t/50)♣	0.18/(1 + 0.14ln(t/50))	Extreme I	[32]

♣ according to service life of 50 years a bias of 1.0 and *CoV* of 0.18 is taken for Live load.

$$p_f = \frac{n_f}{N} \tag{25}$$

The reliability index (β) of the beam sample is obtained from the following equations:

$$\beta = \Phi^{-1}(1 - p_f) \tag{26}$$

where Φ^{-1} is the inverse of standard normal cumulative distribution [18].

The probability distributions of **R**, $\mathbf{Q_{DL}}$, $\mathbf{Q_{LL}}$, **Q**, and scatterplot of **R** versus **Q** corresponding to a sample beam B10_M [35] are presented in Fig. 7. This illustration considers two distinct values of ϕ (0.9 and 0.5) and two different values of α (0.5 and 2.5). This example showcases the computation of the reliability index for the beam, considering various values of α and ϕ ratios. It underscores the dependency of the beam's reliability index on these parameters. The reliability indices of the beam while α varies from 0.5 to 2.5 and ϕ is equal to 0.9 corresponds to reliability indices of 1.21 and 1.58, respectively. The reliability indices corresponding to ϕ of 0.5 are 3.92 ($\alpha = 0.5$) and 3.75 ($\alpha = 2.5$). As expected, increase in ϕ value leads to an increase in the reliability index. While the effect of α on reliability index depends on the value of ϕ. As ϕ value decreases, the **R** and **Q** distribution diverge, and increase in α leads to a larger p_f. On the contrary when **R** and **Q** distribution approach each other, increase in α results in a smaller p_f. This is primarily attributed to the fact that when larger values of α is used, the distribution of **Q** exhibits an elongated upper tail. This elongation is attributed to a greater influence from the $\mathbf{Q_{LL}}$ distribution, characterized by an extreme type I distribution with a large *CoV*. Conversely, when smaller α (0.5) is used, the **Q** distribution tends to resemble a normal distribution, primarily influenced by the $\mathbf{Q_{DL}}$ distribution.

Fig. 8 presents the average reliability indices of all 100 generated sample beams versus ϕ values, corresponding to different values of α. As discussed, an increase in ϕ consistently leads to a decrease in the reliability index. Nevertheless, the influence of α is contingent upon the ϕ value.

To calibrate the resistance reduction factor, the least square method is employed, which allows the determination of the optimal values of the resistance reduction factor that minimizes the difference between the predicted reliability index and the target reliability index:

$$H = \frac{1}{n_{sa}} \sum_{i=1}^{n_{sa}} (\beta_i - \beta_T)^2 \tag{27}$$

where β_i is the reliability index obtained from the analysis and n_{sa} is the total number of scenarios (i.e., 100 beams with 5 different α ratio, resulting 500 scenarios).

As presented in Fig. 9, the values of ϕ corresponding to specific β_T levels were found as follows: for $\beta_T = 3.1$, $\phi = 0.62$; for $\beta_T = 3.4$, $\phi = 0.57$; for $\beta_T = 3.8$, $\phi = 0.52$; and for $\beta_T = 4.1$, $\phi = 0.49$. These calibrated factors can be used in the design process to ensure the desired target reliability levels for shear failure.

5. Validation and discussion

5.1. Construction of dataset

A database comprising 284 RC beams strengthened with EBR-CFRP was constructed from literature [17,34–87], following a filtering process. The filtering criteria involved removing data with: (i) incomplete descriptions of material properties or sectional dimensions; (ii) CFRP shear strength contribution less than or equal to 10 kN; (iii) special configurations other than U-jacketing and fully wrapped; (iv) anchorage systems; (v) special configurations other than CFRP; and (vi) shear span-

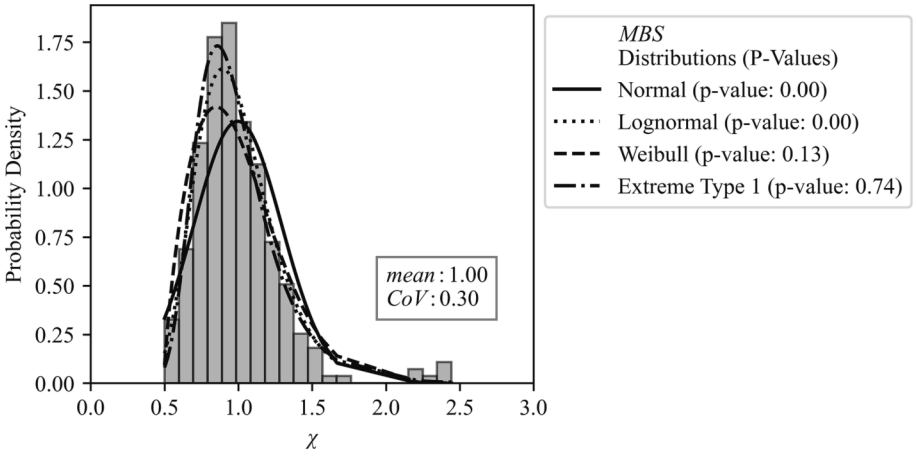

Fig. 6. K-S test result of the model error for MBS model.

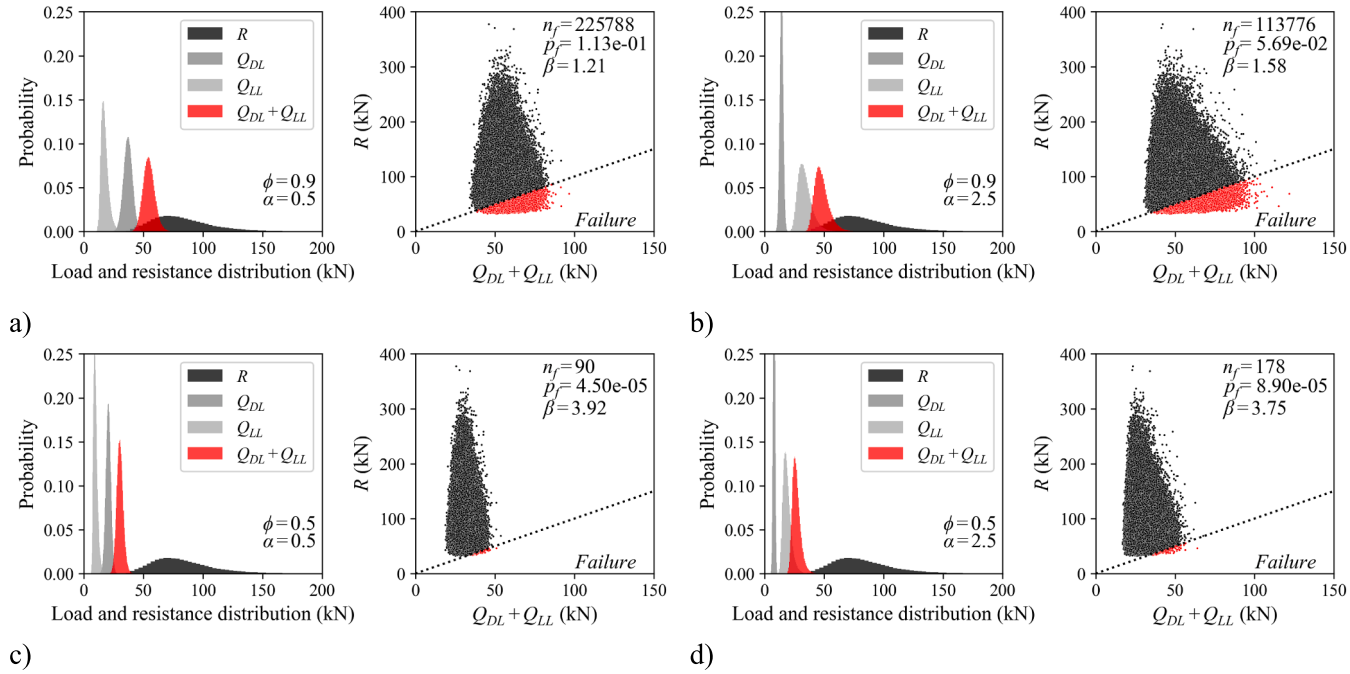

Fig. 7. Reliability analysis of beam B10_M [35] using: a) ϕ = 0.9 and α = 0.5, b) ϕ = 0.9 and α = 2.5, c) ϕ = 0.5 and α = 0.5, d) ϕ = 0.5 and α = 2.5.

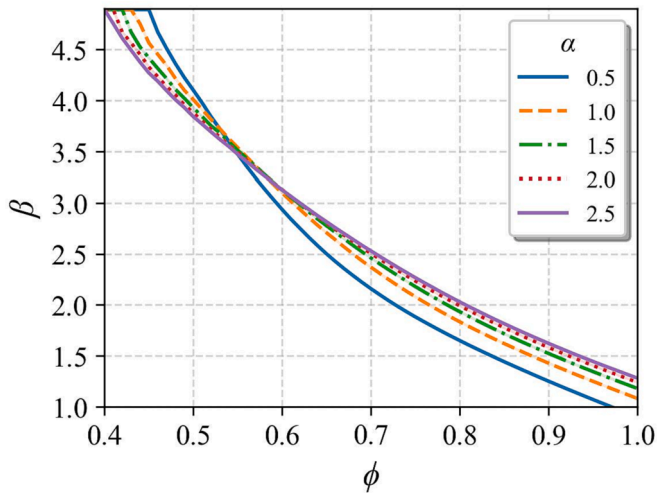

Fig. 8. Average reliability index vs ϕ, corresponding to different α values.

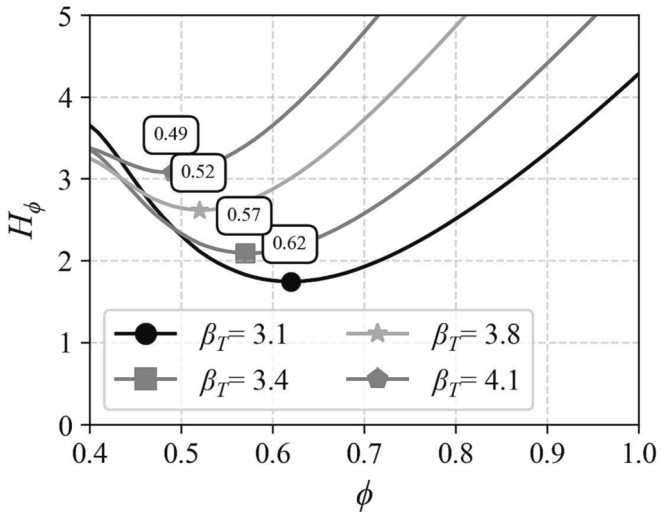

Fig. 9. Average deviation from target reliability index.

to-depth ratios smaller than 2.2. Out of the 284 beams, 211 were strengthened with U-wraps, while the remaining 73 beams were fully wrapped. Furthermore, the database included 202 beams with a rectangular cross-section and 82 beams with a T-section. This database serves as a valuable resource for validating both the proposed and existing models for RC beams strengthened with EBR-CFRP.

5.2. Assessment of models

In this section, the performance of the proposed model is assessed considering Eqs. (14) and (15) for ζ_{MBS} and θ_{MBS}, respectively. In accordance with MC2010 [26], the target reliability index of 3.8 is recommended for the design of new elements with a medium consequence of failure and a service life of 50 years. Hence, in this section, the resistance reduction factor ϕ = 0.52 was utilized to facilitate a comparison of the proposed model's performance with existing design models. However, when considering strengthening purposes, resistance reduction factors are available for various reliability levels, which can be chosen based on the information provided in Section 3.3.3 of MC2010 [26]. It should be emphasized that in the case of ACI 440-2R-17 [22], the shear strength contribution of concrete and steel is determined based on ACI 318-19 [28], and the design value incorporates the corresponding resistance reduction factor. In contrast, as recommended in *fib* bulletin 90 and TR55, Eurocode 2 (EC2) [90] is utilized to evaluate the shear contribution of the steel and concrete components in these models, considering the appropriate partial reduction factors of each models (refer to Appendix A, for more details).

Fig. 10 presents the comparison between the predictions of the proposed model and other existing design models with the experimentally measured values, using the data from the collected database, previously described. The primary objective of design models is to ensure safe predictions. The comparison of the predictions made by the models in Fig. 10 shows that each model has relatively addressed this goal, as there are only a few instances of unsafe predictions observed for each

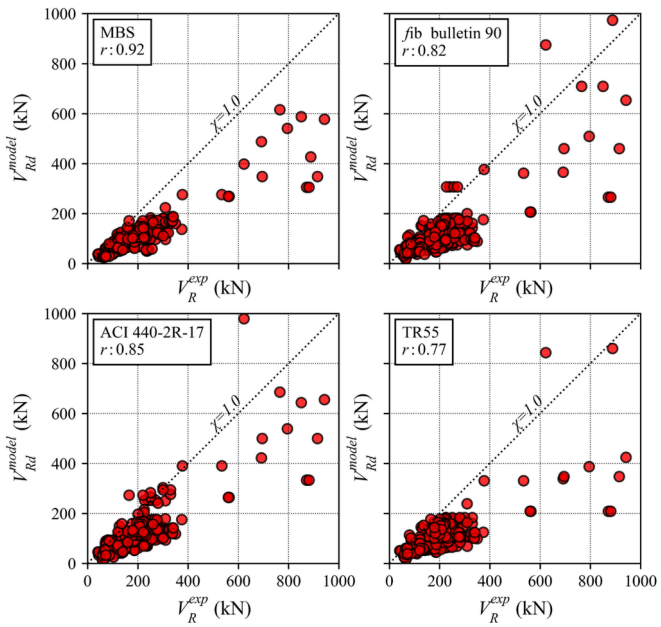

Fig. 10. Predicted versus actual shear resistance of RC beams strengthened with EBR-CFRP.

model. However, in addition to safety, a reliable model should exhibit low dispersion in its predictions, which can be assessed using previously introduced error metrics. The results demonstrate that the proposed model exhibits the least dispersion, as evidenced by its high Pearson correlation coefficient (r) of 0.92. Comparatively, the ACI 440-2R-17 and *fib* bulletin 90 design models also show relatively low dispersion, with r of 0.85 and 0.82, respectively, while the TR55 model presented the highest dispersion, with r of 0.77. To further analyse, the bias and dispersion of each model, the mean, standard deviation (σ) and CoV of model uncertainty ($\chi = V_R^{exp}/V_{Rd}^{model}$) were calculated and are presented in Fig. 11. The results reveal that the proposed design model exhibit less underestimated predictions on average (1.91), its predictions have less dispersion (with $\sigma = 0.57$, and $CoV = 0.3$) compared to the existing design models. This indicates a higher level of safety and reliability. These findings highlight the superior performance of the proposed model in terms of both accuracy and precision compared to the existing design models.

5.3. Demerit point score

It should be emphasized that relying solely on descriptive statistics, such as the mean of χ value, may not provide a comprehensive evaluation of the model reliability. Merely considering the mean χ value being closer to 1.0 does not necessarily indicate a better performance of the model, as this model may still produce a significant number of extremely dangerous or overly conservative predictions. Additionally, it is well-established that extremely dangerous or dangerous predictions have more severe consequences compared to conservative predictions [91]. To overcome this limitation, the Demerit Point Scale Methodology, a weighted penalty categorization approach, is employed [10]. This method assigns penalty points to different ranges of χ and calculates the total demerit point score for each model by considering the percentage of χ falling within each range, the assigned demerit points, and normalizing the result. The resulting score ranges from 0 to 10, being the model performance as better as smaller is the score. It is important to note that, in this study, a modified demerit point classification is used as instead of mean values of shear resistance the design values are compared with the experimental values of shear resistance. This classification not only penalizes highly unsafe predictions, but also penalizes overly conservative predictions to in an attempt of considering both safety and cost arguments for the CFRP-based strengthening solutions. Table 3 gives the demerit points assigned to each model, revealing that the proposed model achieves superior performance with a score of 1.57. It is noteworthy that this model demonstrates a favorable outcome with 97 % of predictions falling within a low, appropriate safety and conservative level, indicating its enhanced reliability and cost-efficiency compared to other models.

5.4. Models feature sensitivity analysis

As previously mentioned, the shear mechanism in RC beams is a complex phenomenon influenced by multiple factors. However, existing models have generally overlooked these dependencies. Consequently, the prediction performance of these models can vary significantly when applied to beams with different conditions. Fig. 12 to Fig. 14 present the

Table 3
Demerit point classification.

χ	Classification	Penalty	MBS	*fib* bulletin 90	ACI 440-R2-17	TR55
<0.75	Extremely dangerous	10	0 %[a]	2 %	1 %	1 %
0.75–1.0	Dangerous	5	0 %	4 %	7 %	3 %
1.0–1.25	Low safety	0	7 %	10 %	10 %	8 %
1.25–1.75	Appropriate safety	1	35 %	35 %	30 %	29 %
1.75–3	Conservative	2	55 %	38 %	48 %	49 %
>3	Extremely conservative	4	3 %	11 %	5 %	10 %
Total demerits point score			1.57[b]	1.95	1.91	1.92

[a] : Percentage of specimens with χ laying in the range.
[b] : $((0 \times 10) + (0 \times 5) + (7 \times 0) + (35 \times 1) + (55 \times 2) + (3 \times 4))/100 = 1.57$.

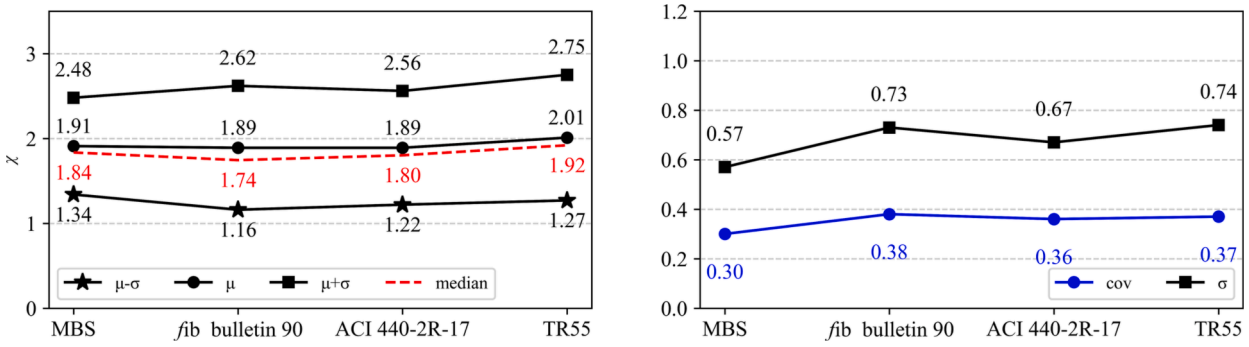

Fig. 11. Statistical analysis of model uncertainties.

boxplots of model uncertainties (for the proposed model and the considered existing design models) with a black line in the boxes that shows the median of χ corresponding to beams with different cross-section shapes (T-section or Rectangular), equivalent transversal reinforcement ($\rho_{sw}+\rho_f E_f/E_{sw}$; where E_{sw} is elastic modulus of steel stirrups), and the ratio of longitudinal reinforcement to the spacing of stirrups (ρ_{sl}/s_s). To quantify the performance of each model a baseline value (a value of 1.84 is used which is the median of χ for all models' predictions) is introduced. Then, the cumulative deviation of medians for each model from this baseline is measured across all input parameter ranges which provides an indication of the model's performance in the proposed analysis (Table 4).

Fig. 12 reveals a considerable underestimation in shear resistance of RC beams with a T-section using the existing models, which may be attributed to their disregard for the contribution of the beam flange and its impact on θ. The cumulative deviations of median values of χ from the baseline were assessed for Rectangular and T-shaped beams. The MBS model exhibited superior performance (0.097) in comparison to *fib* Bulletin 90 (0.457), ACI 440-R2-17 (0.523), and TR55 (0.431). Fig. 13 demonstrates the large variability in predictions among the current models concerning the impact of $\rho_{sw}+\rho_f E_f/E_{sw}$ on the shear resistance, which can be attributed to the omission of ρ_{sw} and ρ_f effect on θ (see Fig. 3). Assessing the cumulative deviations of median χ values from the baseline across various ranges of $\rho_{sw}+\rho_f E_f/E_{sw}$, the MBS model (0.316) outperforms other models such as *fib* Bulletin 90 (1.140), ACI 440-R2-17 (1.218), and TR55 (1.277). Additionally, Fig. 14 illustrates the existing models' tendency to underestimate the shear resistance of beams with the increase of ρ_{sl}/s_s. This is due to the increase of the dowel action with increase of ρ_{sl} and the decrease of the stirrup spacing s_s, which is not accounted by existing models in the parcel corresponding to the CFRP shear contribution. Comparing the cumulative deviations of χ medians from the baseline along different ranges of ρ_{sl}/s_s, the MBS model (0.541) demonstrates superior performance compared to other models, including *fib* Bulletin 90 (1.406), ACI 440-R2-17 (0.870), and TR55 (1.497). Fig. 12 to Fig. 14 demonstrate that the proposed model, which incorporates the influence of cross-section type, equivalent transversal reinforcement, and longitudinal reinforcement, shows improved performance in generating less variation in predictions compared to the baseline value.

6. Conclusion

The study presented in this paper aimed to develop a comprehensive design model for predicting the shear resistance of RC beams strengthened with EBR-CFRP reinforcement, applicable to U-jacketing and fully wrapped configurations. This was achieved by integrating the SMCFT approach and Mohammadi *et al.*'s [10] model, followed by conducting a reliability analysis. A key aspect of the model development was the utilization of a global sensitivity analysis to derive non-iterative prediction equations for two important model parameters: the tensile stress factor in cracked concrete (ζ) and the inclination of the diagonal compressive stress in the web of the section (θ). Furthermore, a Monte Carlo reliability analysis was employed to determine the resistance reduction factor for the model.

To validate the proposed model, a thorough literature review was conducted, resulting in the compilation of a comprehensive database comprising 284 beams strengthened with EBR-CFRP reinforcement. This database served as the basis for comparing the performance of the proposed model against existing design models. Based on the results and discussions presented in this paper, the following conclusions can be drawn:

1- The proposed non-iterative equations for the parameters ζ and θ demonstrate a close resemblance to the values obtained from the SMCFT. The approximate equation for ζ exhibits an *RMSE* of 0.013, a *MAPE* of 4.60 %, an R^2 of 0.96, and an r of 0.98. Similarly, the approximate equation for θ yields an *RMSE* of 1.71, a *MAPE* of 3.51 %, an R^2 of 0.86, and an r of 0.93. These statistical measures indicate the strong agreement between the proposed equations and the SMCFT-based values, validating the accuracy and reliability of the non-iterative approach;
2- The proposed model exhibited superior predictive performance in estimating the shear resistance of RC beams strengthened with EBR-CFRP reinforcement, with r of 0.92;
3- Among the design models considered in this study, the proposed model exhibited the model uncertainties closest to unity, indicating more balanced and less biased predictions. Furthermore, the coefficient of variation (*CoV*) of the proposed model was 0.3, being the lowest one, indicating the proposed model provides more consistent and reliable estimates of shear resistance, making it a favourable choice for practical applications;
4- The reliability analysis conducted in this study reveals that different target reliability indices (β_T) can be achieved by employing specific resistance reduction factors (ϕ). Specifically, a target reliability index of 3.1 corresponds to a resistance reduction factor of 0.62, while indices of 3.4, 3.8 and 4.1 are associated with reduction factors of 0.57, 0.52, and 0.49, respectively;
5- According to the modified demerit point scale methodology performed in this study, the proposed model produces the most reliable and cost-effective predictions in comparison with the considered design models;
6- The considered existing design models overlook dependencies of shear resistance to a few crucial parameters, resulting in varied prediction performance for different beam conditions. The proposed model incorporates effects of several parameters including cross-section type, equivalent transversal reinforcement, and

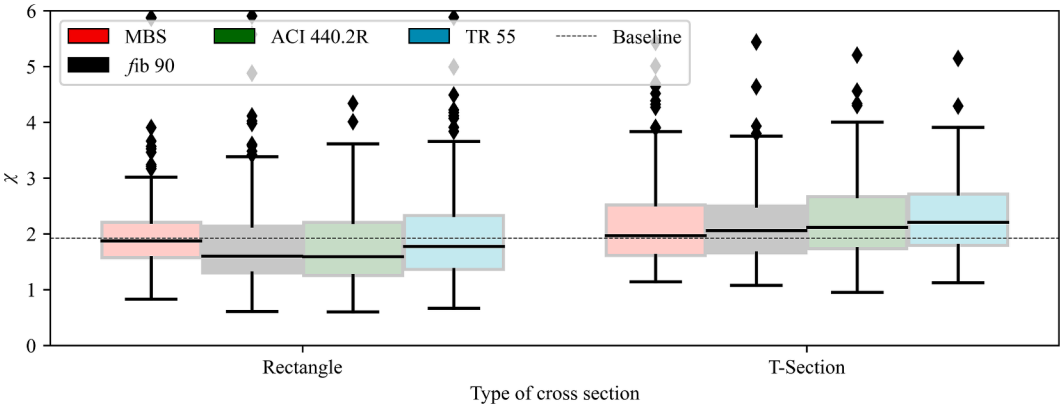

Fig. 12. Prediction performance of models for beams with different cross-section.

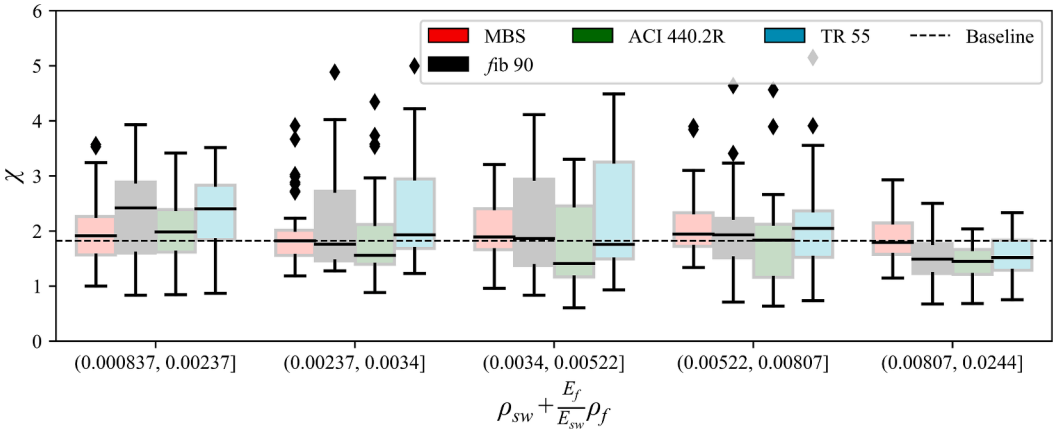

Fig. 13. Prediction performance of models for beams with different equivalent transversal reinforcement.

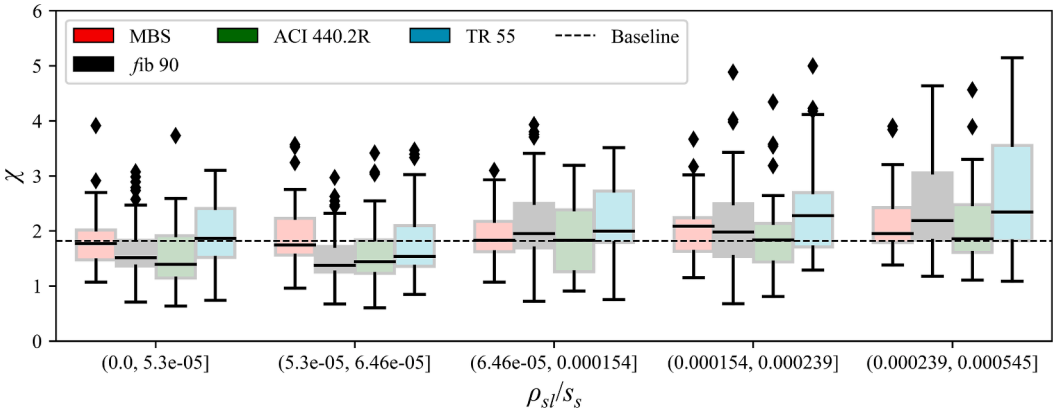

Fig. 14. Prediction performance of models for beams with different ρ_{sl}/s_s.

Table 4
Cumulative deviations of the median values of χ for each model relative to the baseline across different input parameter ranges.

	Models			
Input parameter	MBS	*fib* bulletin 90	ACI 440-R2-17	TR55
Type of cross-section	0.097	0.457	0.523	0.431
$\rho_{sw}+\rho_f E_f/E_{sw}$	0.316	1.140	1.218	1.277
ρ_{sl}/s_s	0.541	1.406	0.870	1.497

longitudinal reinforcement, enhancing its ability to generate less biased predictions for these parameters.

Declaration of competing interest

The authors declare that they have no known competing financial interests or personal relationships that could have appeared to influence the work reported in this paper.

Data availability

Data will be made available on request.

Acknowledgements

This study is a part of the project "Sticker –Innovative technique for the structural strengthening based on using CFRP laminates with multifunctional attributes and applied with advanced cement adhesives", with the reference POCI-01-0247-FEDER-039755. The first author also acknowledges the support provided by FCT PhD individual fellowship with the reference of 2020.08876.BD. This work was partly financed by FCT / MCTES through national funds (PIDDAC) under the R&D Unit Institute for Sustainability and Innovation in Structural Engineering (ISISE), under reference UIDB/04029/2020 (doi.org/10.54499/UIDB/04029/2020), and under the Associate Laboratory Advanced Production and Intelligent Systems ARISE under reference LA/P/0112/2020.

Declaration of generative AI and AI-assisted technologies in the writing process

During the preparation of this work the authors used ChatGPT in order to improve the readability. After using this tool, the authors reviewed and edited the content as needed and takes full responsibility for the content of the publication.

Appendix A. Formulations of design guidelines

Fib bulletin 90

$$V_{Rd} = V_{Rd,sc} + V_{Rd,f} \leqslant V_{Rd,\max} \tag{A1}$$

$$V_{Rd,sc} = \begin{cases} \left[C_{Rd,c}k(100\rho_{sl1}f_{ck})^{\frac{1}{3}} + k_1\sigma_{cp}\right]b_w d_s & \text{where } \rho_{sw} = 0 \\ \dfrac{1}{\gamma_s}0.9d_s\dfrac{A_{sw}}{s_s}f_{swy} & \text{where } \rho_{sw} \neq 0 \end{cases}$$

$$\rho_{sl1} = A_{s1}/(b_w d_s) \tag{A2}$$

$$V_{Rd,\max} = \alpha_{cw}b_w z\nu_1 f_{cd}/(\cot\theta + \tan\theta) \tag{A3}$$

($C_{Rd,c}$, k, k_1,ν_1, α_{cw} are introduced in EN 1992-1-1:2004), σ_{cp} is the stress due to axial load.

$$V_{Rd,f} = A_{fwc}h_{fe}f_{fwd}\left(\cot\theta + \cot\alpha_f\right)\sin\alpha_f$$

where,

$$A_{fw} = 2w_f t_f \quad t_f = \begin{cases} t_0 n_f & \text{if } n_f < 4 \\ t_0\left(n_f\right)^{0.85} & \text{if } n_f \geqslant 4 \end{cases}$$

$$A_{fwc} = \begin{cases} \dfrac{A_{fw}}{s_f} & \text{if strips of FRP are used.} \\ 2t_f\sin\alpha_f & \text{if continuous FRP are used.} \end{cases} \tag{A4}$$

$h_{fe} = \min(h_f, h - 0.1d_s)$ t_0 : thickness of each layer; (n_f in here is the number of FRP layers).

Fully wrapped:$f_{fwd} = f_{fwd,c} = a_t k_R f_{fd}$

U-wrapped:$f_{fwd} = \min\left(f_{fbwd}, f_{fwd,c}\right)$

$$f_{fbwd} = \begin{cases} \left[1 - \dfrac{1}{3}\dfrac{l_e}{\left(h_{fe}/\sin\alpha_f\right)}\right]\dfrac{f_{fbk}}{\gamma_{fb}} & for\ x \geqslant l_e \\ f_{fbwd} = \dfrac{2}{3}\dfrac{h_{fe}/\sin\alpha_f}{l_e}\dfrac{f_{fbk}}{\gamma_{fb}} & for\ x \leqslant l_e \end{cases}$$

$$f_{fbwd} = \begin{cases} \dfrac{f_{fbk}}{\gamma_{fb}} & for\ x \geqslant l_e;\ and\ \ l_e \leqslant y \leqslant x \\ \left[1 - \left(1 - \dfrac{2}{3}\dfrac{ms_f}{l_e}\right)\dfrac{m}{n}\right]\dfrac{f_{fbk}}{\gamma_{fb}} & for\ x \geqslant l_e;\ and\ y \leqslant l_e \\ \dfrac{2}{3}\dfrac{\left(ns_f\right)/\left[\left(\cot\theta + \cot\alpha_f\right)\sin\alpha_f\right]}{l_e}\dfrac{f_{fbk}}{\gamma_{fb}} & for\ x \leqslant l_e;\ and\ \ y \leqslant x \end{cases}$$

$$x = h_{fe}/\sin\alpha_f \qquad l_e = \frac{\pi}{2}\sqrt{\frac{E_f t_f s_{0k}}{\tau_{b1k}}} \qquad k_R = \begin{cases} 0.5\dfrac{R_c}{50}\left(2 - \dfrac{R_c}{50}\right) & R_c < 50\,mm \\ 0.5 & R_c \geqslant 50\,mm \end{cases}$$

$$y = s_f/\left(\cot\theta + \cot\alpha_f\right)\sin\alpha_f \qquad \tau_{b1k} = 0.44\sqrt{f_{cm}f_{ctm}}$$

$$n = int\left[h_{fe}\left(\cot\theta + \cot\alpha_f\right)/s_f\right] \qquad s_{0k} = 0.23$$

$$m = int\left[l_e\left(\cot\theta + \cot\alpha_f\right)\sin\alpha_f/s_f\right] \qquad f_{fbk} = \sqrt{\frac{E_f s_{0k}\tau_{b1k}}{t_f}} \qquad a_t = 0.8,\ f_{fd} = \frac{f_{fu}}{\gamma_f}\ \ \left(\gamma_f = 1.25\right)$$

$$\gamma_{fb} = 1.5 \tag{5}$$

ACI 440-2R-17

$$V_{Rd} = \phi\left[\left(0.17\sqrt{f_c^{'}} + \rho_{sw}f_y\right)b_w d_s + V_f\right] \tag{A6}$$

$$V_f = \psi_f\left(\frac{A_{fv}f_{fe}d_{fv}\left(\sin\alpha_f + \cos\alpha_f\right)}{s_f}\right)$$

where,

$$A_{fv} = 2t_f w_f$$

$$\phi = 0.75, \psi_f = \begin{cases} 0.95 & \text{Fully - wrapped} \\ 0.85 & \text{U - shaped} \end{cases} \quad \text{(A7)}$$

$$f_{fe} = E_f \varepsilon_{fe} \quad \text{(A8)}$$

TR 55

$$V_{Rd} = V_{Rd,sc} + V_{Rd,f} \leqslant V_{Rd,\max} \quad \text{(A9)}$$

$V_{Rd,sc}$ is obtained according to Eq. (A- 2)

$$V_{Rd,f} = \frac{A_{fw}}{s_f}\left(d_{fv} - \frac{n_{ss}}{3} l_{t,\max}\cos\alpha\right) E_{fd}\varepsilon_{fse}\left(\sin\alpha_f + \cos\alpha_f\right) \quad \text{A10)}$$

where,

$$n_{ss} = \begin{cases} 0 & \text{, fully - wrapped} \\ 1 & \text{, U - wrapped} \end{cases} \quad A_{fw} = 2nt_f w_f l_{t,\max} = 0.7\sqrt{\frac{E_{fd}t_f}{f_{ctk}}}$$

$$E_{fd} = \frac{E_{fk}}{\gamma_{FRP,mE}} \varepsilon_{fse} = \min\left\{\varepsilon_{fd} \Big/ 2, 0.5\sqrt{\frac{f_{ctk}}{E_{fd}t_f}}, 0.004\right\} \varepsilon_{fd} = \frac{\varepsilon_{fk}}{\gamma_{FRP,m\varepsilon}}$$

For continuous sheets

$w_f = \sin\alpha_f$, and $s_f = 1$

(Assuming CFRP sheet for shear intervention, partial safety factors for young's module, strain at the ultimate, and manufacturing method are obtained from the guideline.

$\gamma_{FRP,E} = 1.1,\ \gamma_{FRP,\varepsilon} = 1.25,\ \gamma_{FRP,m} = 1.2$

Appendix B. Summary of experimental and analytical results for the compiled dataset

#	ref	Specimen	$V_{R,f}^{exp}$(kN)	V_{Rd}^{MBC}(kN)	$V_{Rd}^{fib\ b90}$(kN)	$V_{Rd}^{ACI440-2R}$(kN)	V_{Rd}^{TR55}(kN)
1	[17]	M1-a	349.4	160.6	88.9	118.2	99.4
2	[17]	M1-b	324.7	169.9	97.8	134.6	118.9
3	[17]	H1-a	333.8	169.9	90.1	119.9	100.6
4	[17]	H1-b	335.8	188.2	102.8	141.7	123.8
5	[17]	H2-a	338.1	169.9	90.1	119.9	100.6
6	[17]	H2-b	340.4	188.2	102.8	141.7	123.8
7	[36]	S3	101.1	79.4	72.8	59.8	71.3
8	[36]	S5	99.1	85.9	93.7	75.8	90.6
9	[37]	CS1	214.0	119.5	120.3	102.2	109.1
10	[37]	CS2	159.0	107.0	93.6	82.4	88.0
11	[37]	CS3	116.0	61.2	60.3	52.5	54.7
12	[38]	A2	185.0	61.9	46.5	52.3	45.5
13	[38]	A3	187.0	61.9	46.5	52.3	45.5
14	[39]	A-SW3-2	177.0	122.6	150.2	159.6	162.8
15	[39]	A-SO3-2	131.0	57.0	62.3	44.5	56.8
16	[39]	A-SO3-3	133.5	60.6	76.7	53.5	68.3
17	[39]	A-SO3-4	144.5	65.8	100.0	71.5	91.4
18	[39]	A-SO3-5	169.5	73.2	123.9	91.8	118.4
19	[39]	A-SO4-2	127.5	57.2	62.5	44.8	57.1
20	[39]	A-SO4-3	155.0	66.0	100.1	72.0	92.0
21	[39]	B-CW2	214.0	130.1	178.4	176.8	173.6
22	[39]	B-CO2	88.0	50.5	56.6	38.6	52.5
23	[39]	B-CO3	113.0	58.2	88.9	61.4	84.8
24	[39]	B-CF2	119.0	61.6	99.1	83.4	91.1
25	[39]	B-CF3	131.0	68.6	150.3	127.3	138.5
26	[39]	B-CF4	140.0	76.1	99.1	89.2	91.1
27	[39]	C-BT2	155.0	97.0	115.8	90.4	105.4
28	[39]	C-BT3	157.5	103.6	142.3	116.4	140.0
29	[39]	C-BT4	162.0	89.4	74.4	60.8	70.2

(*continued on next page*)

(*continued*)

#	ref	Specimen	$V_{R,f}^{exp}$(kN)	V_{Rd}^{MBC}(kN)	$V_{Rd}^{fib\ b90}$(kN)	$V_{Rd}^{ACI440-2R}$(kN)	V_{Rd}^{TR55}(kN)
30	[40]	T4S2-C45	219.1	98.1	64.3	94.7	63.1
31	[41]	T6NS-C45	213.6	139.2	102.4	94.1	101.8
32	[41]	T6S4-C90	272.8	133.8	90.3	113.1	91.1
33	[42]	JS2A	237.1	50.5	76.3	70.1	80.0
34	[42]	JS2B	234.2	50.5	76.3	70.1	80.0
35	[42]	JS4A	243.1	53.8	94.2	87.2	102.9
36	[43]	5	120.1	63.9	88.3	79.2	81.3
37	[43]	6	107.2	65.1	69.9	74.5	–
38	[43]	2	64.5	27.1	61.8	39.3	58.8
39	[43]	3	44.5	28.7	43.1	33.2	–
40	[44]	V10_A	107.0	49.4	54.1	42.1	52.5
41	[44]	V10_B	106.0	49.4	54.1	42.1	52.5
42	[44]	V17_A	103.0	49.4	54.1	42.1	52.5
43	[44]	V11_A	98.0	49.4	54.1	42.1	52.5
44	[44]	V11_B	124.8	49.4	54.1	42.1	52.5
45	[44]	V17_B	92.9	49.4	54.1	42.1	52.5
46	[44]	V12_A	116.0	59.2	54.1	44.0	52.5
47	[44]	V18_A	127.0	59.2	54.1	44.0	52.5
48	[44]	V20_A	140.1	59.2	54.1	44.0	52.5
49	[44]	V12_B	101.7	54.2	54.1	42.1	51.2
50	[44]	V14_B	91.7	54.2	54.1	42.1	51.2
51	[44]	V19_A	118.0	54.2	54.1	42.1	51.2
52	[44]	V19_B	115.1	54.2	54.1	42.1	51.2
53	[44]	V15_B	138.4	54.6	75.3	58.7	72.2
54	[44]	V16_B	112.0	54.6	75.3	58.7	72.2
55	[44]	V16_A	184.0	67.2	75.3	62.6	72.2
56	[44]	V18_B	202.4	67.2	75.3	62.6	72.2
57	[45]	SB3-90	231.5	131.0	181.7	175.5	138.3
58	[45]	SB4-90	217.5	131.0	181.7	175.5	138.3
59	[45]	SB5-90	234.5	131.0	181.7	175.5	138.3
60	[45]	SB6-90	218.0	131.0	181.7	175.5	138.3
61	[45]	SB7-90-0	241.0	144.0	307.1	252.6	176.2
62	[45]	SB8-90-0	227.0	144.0	307.1	252.6	176.2
63	[45]	SB9-45	264.5	135.7	181.7	175.5	138.3
64	[45]	SB10-45	273.5	135.7	181.7	175.5	138.3
65	[45]	SB11-45	254.5	135.7	181.7	175.5	138.3
66	[45]	SB12-45	265.5	135.7	181.7	175.5	138.3
67	[45]	SB13-45-0	256.5	150.7	307.1	252.6	176.2
68	[45]	SB14-45-0	271.0	150.7	307.1	252.6	176.2
69	[46]	US-2	87.5	39.3	47.3	46.3	44.0
70	[46]	US-3	86.3	39.3	47.3	46.3	44.0
71	[46]	US-4	85.0	39.3	47.3	46.3	44.0
72	[46]	UW-2	90.0	41.9	66.0	63.4	68.9
73	[46]	UW-3	88.8	41.9	66.0	63.4	68.9
74	[46]	UW-4	88.8	41.9	66.0	63.4	68.9
75	[47]	C-1	165.0	139.8	146.1	106.0	128.4
76	[47]	C-4	250.0	183.7	158.3	115.2	131.2
77	[48]	case2	212.3	159.8	134.9	129.2	126.7
78	[48]	case3	253.0	168.9	149.7	139.2	137.3
79	[48]	case4	263.0	172.7	157.1	144.2	142.6
80	[48]	case5	293.6	176.2	164.5	149.2	148.0
81	[49]	SB_S0_05L	102.4	76.0	63.0	46.7	58.0
82	[49]	SB_S0_1L	120.0	80.0	81.9	54.8	73.0
83	[49]	SB_S0_2L	121.7	85.4	98.2	67.2	91.5
84	[49]	SB_S1_05L	282.0	147.5	126.4	144.7	121.4
85	[49]	SB_S2_1L	309.4	224.0	199.9	250.9	238.7
86	[50]	SB-S0-1L	59.3	29.8	29.8	16.0	26.3
87	[50]	SB-S0-2L	68.5	32.0	43.7	23.2	37.4
88	[50]	SB-S1-2L	105.1	43.5	49.0	42.9	42.7
89	[51]	UW90	141.5	74.9	71.5	76.2	69.7
90	[51]	2	82.6	52.6	45.5	47.8	46.5
91	[51]	3	82.0	52.0	42.8	45.8	43.6
92	[52]	RS4W	250.0	152.9	143.1	264.9	159.6
93	[52]	RS3W	330.0	161.1	143.1	276.3	159.6
94	[52]	RS2W	300.0	180.4	154.6	302.9	171.2
95	[52]	RS4Wa	250.0	173.1	160.9	282.9	183.2
96	[52]	RS3Wa	330.0	180.7	160.9	294.2	183.2
97	[52]	RS2Wa	300.0	180.7	160.9	294.2	183.2
98	[52]	RS3Ua	225.0	153.8	160.9	215.4	183.2
99	[52]	RS2Ua	280.0	173.0	161.2	241.6	183.5
100	[52]	RS4Ub	225.0	145.7	160.9	204.1	183.2
101	[53]	BT1-1	67.0	42.3	52.8	43.2	50.4
102	[53]	BT1-1I	87.0	42.3	52.8	43.2	50.4
103	[53]	BT1-2I	67.4	37.4	43.0	38.9	41.2
104	[53]	BS1-1	61.0	38.8	48.8	43.2	46.4
105	[53]	BS1-2	51.0	40.8	47.0	38.9	45.3

(*continued on next page*)

(*continued*)

#	ref	Specimen	$V_{R,f}^{exp}$(kN)	V_{Rd}^{MBC}(kN)	$V_{Rd}^{fib\ b90}$(kN)	$V_{Rd}^{ACI440-2R}$(kN)	V_{Rd}^{TR55}(kN)
106	[54]	S0-US	377.0	276.5	377.2	390.1	330.5
107	[54]	S0-UA	534.0	276.5	362.1	390.1	330.5
108	[54]	S0-CS	695.0	348.3	460.3	499.6	347.4
109	[54]	S0-CA	915.0	348.3	460.3	499.6	347.4
110	[54]	S5-UA	622.0	398.3	875.3	979.0	843.7
111	[54]	S5-CA	888.0	426.7	973.4	1088.5	860.6
112	[55]	G1-B	72.7	62.0	106.9	89.9	–
113	[55]	G2-B-N8	80.7	62.9	83.2	93.8	–
114	[55]	G2-B-N6	70.0	60.8	56.6	79.0	–
115	[55]	G3-MB-N8-P1	94.0	62.2	80.6	92.5	–
116	[55]	G3-B-N6	74.0	59.0	51.8	75.9	–
117	[56]	RB200C	97.8	36.9	43.4	35.2	45.9
118	[56]	RB150C	101.0	38.2	48.5	39.8	51.9
119	[57]	S3-EB-NA	243.2	118.4	129.1	119.2	104.2
120	[57]	S3-EB	222.0	135.8	117.1	137.7	110.5
121	[58]	SB-U1	65.0	24.1	18.7	21.9	18.4
122	[58]	SB-F1	66.1	27.3	20.7	24.7	18.4
123	[58]	SB-F2	66.7	27.3	20.7	24.7	18.4
124	[58]	MB-F1	236.4	99.8	81.7	96.3	65.2
125	[58]	MB-F2	250.3	99.8	81.7	96.3	65.2
126	[58]	LB-U1	563.4	268.6	206.2	264.0	208.7
127	[58]	LB-U2	559.8	268.6	206.2	264.0	208.7
128	[58]	LB-F1	871.6	305.8	265.8	333.6	208.7
129	[58]	LB-F2	881.2	305.8	265.8	333.6	208.7
130	[59]	RC-8-S90-	850.0	588.2	709.5	643.9	–
131	[59]	RC-12-S90-	765.0	615.5	709.5	685.6	–
132	[61]	ED1-S0-0.5L	102.0	77.1	67.2	48.5	59.7
133	[61]	ED1-S0-1L	120.0	81.4	82.5	57.8	76.0
134	[61]	ED1-S0-2L	122.0	87.3	98.2	71.1	96.1
135	[61]	ED1-S1-0.5L	282.0	117.2	91.2	108.8	83.8
136	[61]	ED1-S2-1L	309.0	167.6	169.5	178.4	163.0
137	[61]	ED2-S0-1L	59.0	26.5	30.9	13.6	24.9
138	[61]	ED2-S0-2L	68.0	28.5	37.9	19.6	35.6
139	[61]	ED2-S1-2L	105.0	42.4	46.7	41.3	44.4
140	[61]	U90S5-a(L)	246.7	135.3	–	158.0	146.3
141	[61]	U90S5-b(L)	235.9	123.1	–	139.9	131.4
142	[61]	U90C5-a(L)	217.0	124.4	167.2	161.5	163.9
143	[61]	U90C5-b(L)	243.3	121.1	161.3	155.8	158.6
144	[61]	U45S5(L)	206.2	148.2	177.6	166.7	156.0
145	[61]	W90S5(L)	276.2	137.5	175.8	175.1	124.4
146	[61]	U90S3-a(L)	207.4	104.8	–	113.1	102.1
147	[61]	U90S3-b(L)	203.6	108.0	–	117.4	106.2
148	[61]	U90S3-c(L)	231.8	104.0	–	112.0	100.9
149	[61]	U90C3-a(L)	208.8	125.4	157.8	157.3	151.8
150	[61]	U90c3-b(L)	201.8	125.4	157.8	157.3	151.8
151	[61]	U45S3-a(L)	189.6	119.3	127.5	125.2	114.7
152	[61]	U45S3-b(L)	211.0	136.4	150.8	148.7	136.0
153	[61]	W90S3-a(L)	311.4	123.7	122.6	135.0	106.2
154	[61]	W90S3-b(L)	284.3	123.8	122.7	135.1	106.3
155	[61]	U90S5-a	218.1	135.3	–	158.0	146.3
156	[61]	U90S5-b	225.6	123.1	–	139.9	131.4
157	[61]	U90C5-a	194.5	124.4	167.2	161.5	163.9
158	[61]	U90C5-b	221.9	121.1	161.3	155.8	158.6
159	[61]	U45S5	221.4	148.2	177.6	166.7	156.0
160	[61]	W90S5	374.3	137.5	175.8	175.1	124.4
161	[61]	U90S3-a	195.6	104.8	–	113.1	102.1
162	[61]	U90S3-b	223.9	108.0	–	117.4	106.2
163	[61]	U90S3-c	179.3	104.0	–	112.0	100.9
164	[61]	U90C3-a	215.4	125.4	157.8	157.3	151.8
165	[61]	U90c3-b	204.0	125.4	157.8	157.3	151.8
166	[61]	U45S3-a	198.8	119.3	127.5	125.2	114.7
167	[61]	U45S3-b	207.6	136.4	150.8	148.7	136.0
168	[61]	W90S3-a	321.4	123.7	122.6	135.0	106.2
169	[61]	W90S3-b	276.6	123.8	122.7	135.1	106.3
170	[63]	RS4WL4	220.0	171.7	158.9	272.6	177.0
171	[63]	RS4UL4	200.0	143.8	158.9	196.4	177.0
172	[63]	RS4WL2.5	165.0	171.7	158.9	272.6	177.0
173	[64]	B-7	68.5	40.4	60.2	36.7	53.3
174	[64]	B-8	85.8	44.2	68.1	50.0	65.1
175	[65]	VC 01	110.0	53.5	37.6	45.1	38.5
176	[65]	VC 03	100.0	55.6	44.0	50.6	45.4
177	[65]	VC 07	103.5	62.8	60.9	74.2	–
178	[66]	S0-0.12R	120.9	81.0	56.3	45.4	55.0
179	[66]	S0-0.17R1	134.5	83.4	62.7	50.2	60.8
180	[66]	S0-0.17R2	102.4	88.7	83.6	65.9	79.8
181	[66]	S0-0.20R1	135.7	84.7	67.1	53.5	64.8

(*continued on next page*)

(*continued*)

#	ref	Specimen	$V_{R,f}^{exp}$(kN)	V_{Rd}^{MBC}(kN)	$V_{Rd}^{fib\ b90}$(kN)	$V_{Rd}^{ACI440-2R}$(kN)	V_{Rd}^{TR55}(kN)
182	[66]	S0-0.20R2	131.1	84.7	66.9	53.3	64.6
183	[66]	S0-0.23R	150.6	85.8	71.0	56.5	68.4
184	[66]	S0-0.33R	120.0	88.7	83.6	65.9	79.8
185	[66]	S0-0.66R	121.7	88.7	83.6	65.9	79.8
186	[66]	S1-0.17R1	242.3	138.9	105.9	131.6	104.0
187	[66]	S1-0.17R2	246.7	138.9	105.9	131.6	104.0
188	[66]	S1-0.23R	253.9	140.8	114.2	137.9	111.6
189	[66]	S1-0.33R	250.6	143.1	126.8	147.3	123.0
190	[67]	Beam 2 – CFRP – No anchors	186.5	86.3	74.8	91.1	75.5
191	[68]	JS2A	236.0	54.6	82.7	77.7	86.1
192	[68]	JS2B	233.0	54.6	82.7	77.7	86.1
193	[68]	JS4A	256.0	58.4	102.7	96.9	111.0
194	[70]	C5	135.6	95.6	172.0	158.8	152.6
195	[71]	S00	182.0	111.9	127.2	125.7	120.7
196	[72]	F/295/LP1/4.5	135.0	53.2	63.8	41.5	60.1
197	[72]	F/295/LP1/3.3	122.5	52.2	67.2	44.4	61.0
198	[72]	F/215/LP1/4.6	102.5	42.6	48.3	25.6	41.2
199	[73]	EBL-S0	129.8	102.2	64.3	60.2	–
200	[73]	EBL-S1	260.3	164.9	121.5	156.7	–
201	[73]	EBL-S3	221.9	140.9	88.6	125.2	–
202	[74]	SB_R1	60.2	28.5	43.2	33.0	38.8
203	[74]	SB_R2	65.0	32.1	70.6	54.5	59.9
204	[74]	UW_R1	86.1	29.6	43.7	33.4	39.2
205	[74]	UW_R2	71.3	33.4	71.1	55.0	60.9
206	[74]	FW_R1	72.3	28.5	43.2	33.0	38.8
207	[75]	C1-EB1	120.0	60.6	58.9	56.6	51.9
208	[75]	C2-EB2	107.2	63.4	48.2	65.9	–
209	[75]	C2-EB2R	116.0	63.4	48.2	65.9	–
210	[75]	C2-EB3	120.0	64.1	48.2	72.7	–
211	[76]	S0-U	223.7	103.9	95.5	70.1	–
212	[76]	S8-U	300.8	111.2	95.5	101.4	–
213	[77]	TB2	140.0	54.5	36.8	46.9	–
214	[78]	BSU	159.3	98.1	90.2	84.9	–
215	[78]	WBR1	85.5	79.3	78.5	89.4	101.4
216	[78]	WBR2	178.8	102.3	106.5	132.3	143.6
217	[79]	A-U1-C-17	238.1	127.2	125.9	135.7	119.2
218	[79]	A-U1-C-20	225.0	119.8	116.6	126.8	110.0
219	[79]	A-U1-S-17	247.3	127.2	125.9	135.7	119.2
220	[79]	A-U1-S-20	235.1	119.8	116.6	126.8	110.0
221	[79]	A-U2-C-17	243.0	135.8	163.1	158.4	160.3
222	[79]	A-U2-C-20	229.7	128.6	153.8	149.6	151.1
223	[79]	A-U2-S-17	218.9	135.8	163.1	158.4	160.3
224	[80]	S-2	691.5	487.9	365.8	422.3	338.8
225	[80]	S-3	795.0	541.3	509.8	538.8	387.3
226	[80]	S-4	942.0	577.4	653.8	655.4	424.4
227	[81]	2	285.2	142.0	117.1	99.2	110.0
228	[82]	No, 2	223.0	101.1	69.0	83.7	62.8
229	[83]	B10_M	55.6	32.8	31.9	31.6	39.3
230	[83]	B12_M	71.5	40.0	54.2	47.2	60.6
231	[85]	2S_7M(1)	195.1	114.8	83.6	101.7	86.8
232	[85]	2S_7M(2)	222.1	120.9	109.0	113.6	103.5
233	[85]	4S_4M(1)	250.4	124.8	73.1	110.5	75.1
234	[85]	4S_7M(1)	253.8	128.1	83.6	120.2	86.8
235	[86]	UBF-R6	205.5	95.1	60.7	83.7	56.2
236	[86]	BDF-R6	180.9	96.9	61.5	84.8	57.0
237	[86]	UBF-R8	198.3	115.2	88.9	111.3	84.4
238	[86]	BDF-R8	213.6	114.9	88.9	111.1	84.4
239	[87]	1-R1	215.8	133.8	123.6	171.8	111.4
240	[88]	CS.2	100.5	66.4	60.9	43.4	54.8
241	[88]	DS.2	139.0	75.0	61.5	65.7	55.2
242	[89]	B15	86.9	51.1	92.9	69.5	88.2
243	[89]	B16	80.0	56.7	114.3	92.1	113.4
244	[92]	BS2	124.0	116.2	77.4	116.4	76.6
245	[92]	BS4	126.0	121.2	151.2	149.4	145.1
246	[92]	BS7	117.8	117.6	87.9	101.9	86.4
247	[93]	SB1-3	240.0	108.6	138.1	141.1	127.5
248	[93]	SB1-4	253.0	108.6	138.1	141.1	127.5
249	[93]	SB1-5	246.0	96.6	75.4	93.9	69.1
250	[93]	SB1-6	230.0	96.6	75.4	93.9	69.1
251	[93]	SB1-9	240.0	97.5	85.1	103.6	81.2
252	[93]	SB1-10	243.0	97.5	85.1	103.6	81.2
253	[93]	SB2-3	270.0	96.6	75.4	93.9	69.1
254	[93]	SB3-2	310.0	96.6	75.4	93.9	69.1
255	[94]	US60	111.0	93.5	85.9	97.0	–
256	[94]	USVA	120.0	97.5	87.3	97.7	–
257	[94]	USVA+	135.0	93.5	85.9	97.0	–

(*continued on next page*)

(*continued*)

#	ref	Specimen	$V_{R,f}^{exp}$(kN)	V_{Rd}^{MBC}(kN)	$V_{Rd}^{fib\ b90}$(kN)	$V_{Rd}^{ACI440-2R}$(kN)	V_{Rd}^{TR55}(kN)
258	[94]	US45+	126.0	97.5	87.3	97.7	–
259	[94]	UF90	125.0	90.0	90.7	106.8	–
260	[94]	US45++	133.5	125.0	94.7	106.8	–
261	[94]	US45 + A	167.0	93.2	94.7	106.8	–
262	[94]	UF45++B	172.0	93.2	94.7	106.8	–
263	[94]	UF45++C	183.0	93.2	94.7	106.8	–
264	[94]	US45++F	163.5	110.8	94.7	106.8	–
265	[94]	US45++E	150.0	110.8	94.7	106.8	–
266	[94]	US45 + D	164.5	110.8	94.7	106.8	–
267	[94]	WS45++	158.5	145.0	116.1	127.8	–
268	[95]	BT2-1	67.0	35.7	49.4	38.7	47.1
269	[95]	BT2-2	61.0	41.5	59.0	45.8	54.0
270	[95]	BT2-2I	77.0	41.5	59.0	45.8	54.0
271	[95]	BS2-1	54.0	31.6	40.1	34.4	38.4
272	[95]	BS2-2	41.0	38.2	55.4	45.8	50.5
273	[95]	BS2-2I	44.0	38.2	55.4	45.8	50.5
274	[95]	TT1-1	120.6	105.3	107.0	126.1	105.5
275	[95]	TS1-1	94.0	70.3	62.1	83.1	60.5
276	[95]	TS1-2	80.7	69.6	58.2	80.1	57.0
277	[96]	PU1	142.5	59.5	57.7	69.2	59.1
278	[96]	PU2	130.0	58.2	53.7	65.6	54.8
279	[96]	PU3	154.5	64.5	56.6	68.1	56.8
280	[96]	PU4	150.0	63.3	53.9	65.7	54.0
281	[96]	PC1	177.5	68.2	57.7	72.0	59.1
282	[96]	PC2	155.0	66.2	53.7	67.9	54.8
283	[96]	PC3	145.5	75.8	56.6	70.9	57.8
284	[96]	PC4	132.0	73.9	53.9	68.1	54.9

References

[1] Breveglieri M, Aprile A, Barros JAO. RC beams strengthened in shear using the embedded through-section technique: experimental results and analytical formulation. Compos Part B Eng 2016;89:266–81. https://doi.org/10.1016/j.compositesb.2015.11.023.

[2] Dias SJE, Barros JAO. NSM shear strengthening technique with CFRP laminates applied in high T cross section RC beams. Compos Part B Eng 2017;114:256–67. https://doi.org/10.1016/j.compositesb.2017.01.028.

[3] Fib bulletin No. 90. Externally applied FRP reinforcement for concrete structures. Technical report (229 pages, ISBN 978-2-88394-132-8, July 2019). fib. The International Federation for Structural Concrete; 2019. 10.35789/fib.BULL.0090.

[4] Sayed AM, Wang X, Wu Z. Finite element modeling of the shear capacity of RC beams strengthened with FRP sheets by considering different failure modes. Constr Build Mater 2014;59:169–79. https://doi.org/10.1016/j.conbuildmat.2014.02.044.

[5] Zhang Z, Hsu C-T-T. Shear strengthening of reinforced concrete beams using carbon-fiber-reinforced polymer laminates. J Compos Constr 2005;9:158–69.

[6] Perera R, Ruiz A. Design equations for reinforced concrete members strengthened in shear with external FRP reinforcement formulated in an evolutionary multi-objective framework. Compos Part B 2012;43:488–96. https://doi.org/10.1016/j.compositesb.2011.10.013.

[7] Chen GM, Teng JG, Chen JF. Shear strength model for FRP-strengthened RC beams with adverse FRP-steel interaction. J Compos Constr 2013;17:50–66. https://doi.org/10.1061/(asce)cc.1943-5614.0000313.

[8] Colotti V. Mechanical shear strength model for reinforced concrete beams strengthened with FRP materials. Constr Build Mater 2016;124:855–65. https://doi.org/10.1016/j.conbuildmat.2016.07.146.

[9] Mofidi A, Chaallal O. Shear strengthening of RC beams with EB FRP: influencing factors and conceptual debonding model. J Compos Constr 2011;15:62–74. https://doi.org/10.1061/(asce)cc.1943-5614.0000153.

[10] Mohammadi A, Barros JAO, Sena-Cruz J. A new model for predicting the shear strength of RC beams strengthened with externally bonded FRP sheets. Compos Struct 2023;319:117081. https://doi.org/10.1016/j.compstruct.2023.117081.

[11] A. Mohammadi, J.A.O. Barros, J. Sena-Cruz, Performance of models for predicting the shear capacity of FRP-strengthened RC beams 2023. 10.5281/ZENODO.8066241.

[12] Bentz EC, Vecchio FJ, Collins MP. Simplified modified compression field theory for calculating shear strength of reinforced concrete elements. ACI Struct J 2007;104(378–80). https://doi.org/10.14359/16438.

[13] Baghi H, Barros JAO. Design approach to determine shear capacity of reinforced concrete beams shear strengthened with NSM systems. J Struct Eng 2017:143. https://doi.org/10.1061/(asce)st.1943-541x.0001793.

[14] Barros JAO, Foster SJ. An integrated approach for predicting the shear capacity of fibre reinforced concrete beams. Eng Struct 2018;174:346–57. https://doi.org/10.1016/j.engstruct.2018.07.071.

[15] Cladera A, Marí A, Ribas C, Bairán J, Oller E. Predicting the shear-flexural strength of slender reinforced concrete T and I shaped beams. Eng Struct 2015;101:386–98. https://doi.org/10.1016/j.engstruct.2015.07.025.

[16] Baghi H, Barros JAO. Design-oriented approach to predict shear strength of reinforced concrete beams. Struct Concr 2018;19:98–115. https://doi.org/10.1002/suco.201700095.

[17] Oller E, Pujol M, Marí A. Contribution of externally bonded FRP shear reinforcement to the shear strength of RC beams. Compos Part B 2019;164:235–48. https://doi.org/10.1016/j.compositesb.2018.11.065.

[18] Huang X, Sui L, Xing F, Zhou Y, Wu Y. Reliability assessment for flexural FRP-Strengthened reinforced concrete beams based on Importance Sampling. Compos Part B Eng 2019;156:378–98. https://doi.org/10.1016/j.compositesb.2018.09.002.

[19] Zhou Y, Zhang J, Li W, Hu B, Huang X. Reliability-based design analysis of FRP shear strengthened reinforced concrete beams considering different FRP configurations. Compos Struct 2020;237:111957. https://doi.org/10.1016/j.compstruct.2020.111957.

[20] Huang X, Zhou Y, Li W, Hu B, Zhang J. Reliability-based design of FRP shear strengthened reinforced concrete Beams: guidelines assessment and calibration. Compos Struct 2023;323:117421. https://doi.org/10.1016/j.compstruct.2023.117421.

[21] Barros JAO, Lima JLT, Meneguetti V, S.J.E. D, Santos LD. Technical report 11-DEC/E-05: DABASUM – Data base for FRP-based shear strengthening of reinforced concrete beams. Guimaraes, Portugal: 2011.

[22] ACI440.2R-17. Guide for the design and construction of externally bonded FRP systems for strengthening existing structures. 2017.

[23] TR55. Design guidance for strengthening concrete structures using fibre composite materials. third ed. Camberley: Concrete Society; 2012.

[24] RILEM TC 162-TDF. Test and design methods for steel fibre reinforced concrete Recommendations. Mater. Struct., 2000;33:75–81.

[25] Saltelli A, Ratto M, Andres T, Campolongo F, Cariboni J, Gatelli D, et al. Global sensitivity analysis: The primer. 2008. 10.1002/9780470725184.

[26] fib Model Code. Fédération Internationale du Béton (fib), MC2010, Model Code for Concrete Structures 2010. 2010:247–78.

[27] Cabanzo CM, Tinoco J, Sousa HS, Coelho M, Matos JC. Computers and Geotechnics Adaptation of traditional risk-based methodology for slopes to probabilistic-based approach integrating surrogate models. Comput Geotech 2023;161:105577. https://doi.org/10.1016/j.compgeo.2023.105577.

[28] ACI Committee. Building code requirements for structural concrete (ACI 318-19) and commentary; 2019.

[29] Bathurst RJ, Allen TM, Nowak AS. Calibration concepts for load and resistance factor design (LRFD) of reinforced soil walls. Can Geotech J 2008;45:1377–92. https://doi.org/10.1139/T08-063.

[30] Lu R, Luo Y, Conte JP. Reliability evaluation of reinforced concrete beams. Struct Saf 1994;14:277–98. https://doi.org/10.1016/0167-4730(94)90016-7.

[31] Firouz RM, Pereira ENB, Barros JAO. Cementitious adhesives for NSM carbon laminate strengthening system with treated surfaces. IABSE Symp Guimaraes 2019 Towar a Resilient Built Environ Risk Asset Manag - Rep 2019:353–9.

[32] Firouzi A, Taki A, Mohammadzadeh S. Time-dependent reliability analysis of RC beams shear and flexural strengthened with CFRP subjected to harsh environmental deteriorations. Eng Struct 2019;196:109326. https://doi.org/10.1016/j.engstruct.2019.109326.

[33] Pham HB, Al-Mahaidi R. Reliablity analysis of bridge beams retrofitted with fibre reinforced polymers. Compos Struct 2008;82:177–84. https://doi.org/10.1016/j.compstruct.2006.12.010.
[34] Ribeiro SEC, Diniz SMC. Reliability-based design recommendations for FRP-reinforced concrete beams. Eng Struct 2013;52:273–83. https://doi.org/10.1016/j.engstruct.2013.02.026.
[35] Barros JAO, Dias SJE, Lima JLT. Efficacy of CFRP-based techniques for the flexural and shear strengthening of concrete beams. Cem Concr Compos 2007;29:203–17. https://doi.org/10.1016/j.cemconcomp.2006.09.001.
[36] Sato Y, Ueda T, Kakuta Y, Tanaka T. Shear reinforcing effect attached to side of reinforced concrete beams. In: Proc 2nd Int Conf Adv Compos Mater Bridg Struct, MONTREAL; 1996. p. 621–8.
[37] Umezu K, Fujita M, Nakai H, e Tamaki K. Shear behavior of RC beams with aramid fiber sheet, Japan concrete institute, non-metallic(FRP) reinforcement for concrete structures. Proceeding Third Int Symp 1997;1:491–8.
[38] Cao SY, Chen JF, Teng JG, Hao Z, Chen JF. Debonding in RC beams shear strengthened with complete FRP wraps. J Compos Constr 2005;9:417–28. https://doi.org/10.1061/(asce)1090-0268(2005)9:5(417).
[39] Khalifa A. Shear performance of reinforced concrete beams strengthened with advanced composites; 1999.
[40] Deniaud C, Cheng JJR, Asce M. Reinforced concrete T-beams strengthened in shear with FRP sheets. Struct Eng Rep 2003;7:65–88.
[41] Deniaud C, Cheng JJR. Shear behavior of reinforced concrete T-beams with externally bonded fiber-reinforced polymer sheets. ACI Struct J 2001;98(386–94). https://doi.org/10.14359/10227.
[42] Annaiah RH, Myers JJ, Nanni A. Shear Performance of RC BeamsStrengthened In Situ with Composites; 2001.
[43] Park SY, Naaman AE, Lopez MM, Till RD. Shear Strengthening Effect of RC Beams Using Glued CFRP Sheets. FRP Compos. Civ. Eng. Proc. Int. Conf. FRP Compos. Civ. Eng., Hong Kong, China: 2001, p. 668–878.
[44] Beber AJ. Comportamento Estrutural de Vigas de Concreto Armado Reforçadas com Compósitos de Fibra de Carbono. Tese (Doutorado Em Eng - Programa Pós-Graduação Em Eng Civ 2003:317.
[45] Alagusundaramoorthy P, Harik IE, Choo CC. Shear strength of R/C beams wrapped with CFRP fabric. Kentucky 2002.
[46] Allam SM, Ebeido TI. Retrofitting of RC beams predamaged in shear using CFRP sheets. AEJ - Alexandria Eng J 2003;42:87–101.
[47] Adhikary BB, Mutsuyoshi H, Ashraf M, Mutsuyoshi H. Shear strengthening of reinforced concrete beams using fiber-reinforced polymer sheets with bonded anchorage. ACI Struct J 2004;101(660–8). https://doi.org/10.14359/13388.
[48] Miyajima H, Kosa K, Tasaki K, Matsumoto S. Shear strengthening of RC beams using carbon fiber sheets and its resistance mechanism. Proc. Fifth Work. Saf. Stab. Infrastructures against Environ. Impacts, Manila, Philippines: 2005, p. 114–25.
[49] Bousselham A, Chaallal O. Behavior of reinforced concrete T-beams strengthened in shear with carbon fiber-reinforced polymer-an experimental study. ACI Struct J 2006;103:339.
[50] Bousselham A, Chaallal O. Effect of transverse steel and shear span on the performance of RC beams strengthened in shear with CFRP. Compos Part B Eng 2006;37:37–46.
[51] De Lorenzis L, Rizzo A. Behaviour and capacity of RC beams strengthened in shear with NSM FRP reinforcement. 2nd Int. fib Congr., Naples: 2006.
[52] Grande E, Imbimbo M, Rasulo A. Effect of transverse steel on the response of RC beams strengthened in shear by FRP: experimental study. J Compos Constr 2009;13:405–14.
[53] Jayaprakash J, Samad AAA, Abbasovich AA, Ali AAA. Shear capacity of precracked and non-precracked reinforced concrete shear beams with externally bonded bi-directional CFRP strips. Constr Build Mater 2008;22:1148–65.
[54] Colalillo MA, Sheikh SA. Seismic retrofit of shear-critical reinforced concrete beams using CFRP. Constr Build Mater 2012;32:99–109.
[55] Ebead U, Saeed H. Hybrid mechanically fastened/externally bonded FRP for RC beam shear strengthening. Rome, Italy: CICE; 2012.
[56] Katakalos K, Manos GC, Papakonstantinou CG. Comparison between carbon and steel fiber reinforced polymers with or without anchorage. 6th CICE, Rome 2012.
[57] Mofidi A, Chaallal O, Benmokrane B, Neale KW. Performance and comparison of end-anchorage systems for RC beams strengthened in shear with U wrap FRP. 6th CICE, Rome; 2012.
[58] Leung CKY, Chen Z, Lee S, Ng M, Xu M, Tang J. Effect of size on the failure of geometrically similar concrete beams strengthened in shear with FRP strips. J Compos Constr 2007;11:487–96.
[59] Belarbi A, Murphy M, Bae SW. Shear strengthening of full-scale RC T-beams with CFRP sheets. 3rd Asia-Pacific Conf. FRP Struct. APFIS 2012, 2012.
[60] Altin S, Anil Ö, Kopraman Y, Mertoğlu Ç, Kara ME. Improving shear capacity and ductility of shear-deficient RC beams using CFRP strips. J Reinf Plast Compos 2010;29:2975–91.
[61] Bousselham A, Chaallal O. Mechanisms of shear resistance of concrete beams strengthened in shear with externally bonded FRP. J Compos Constr 2008;12:499–512. https://doi.org/10.1061/(asce)1090-0268(2008)12:5(499).
[62] Chaallal O, Mofidi A, Benmokrane B, Neale K. Embedded through-section FRP rod method for shear strengthening of RC beams: performance and comparison with existing techniques. J Compos Constr 2011;15:374–83. https://doi.org/10.1061/(asce)cc.1943-5614.0000174.
[63] Grande E, Imbimbo M, Rasulo A. Experimental response of RC beams strengthened in shear by FRP sheets. Open Civ Eng J 2013;7:127–35. https://doi.org/10.2174/1874149501307010127.
[64] Adhikary BB, Mutsuyoshi H. Behavior of concrete beams strengthened in shear with carbon-fiber sheets. J Compos Constr 2004;8:258–64. https://doi.org/10.1061/(asce)1090-0268(2004)8:3(258).
[65] Gamino AL. Modelagem física e computacional de estruturas de concreto reforçadas com CFRP; 2007.
[66] Mofidi A, Chaallal O. Shear strengthening of RC beams with externally bonded FRP composites: effect of strip-width-to-strip-spacing ratio. J Compos Constr 2011;15:732–42. https://doi.org/10.1061/(ASCE)CC.1943-5614.0000219.
[67] Baggio D, Soudki K, Noël M. Strengthening of shear critical RC beams with various FRP systems. Constr Build Mater 2014;66:634–44. https://doi.org/10.1016/j.conbuildmat.2014.05.097.
[68] Micelli F, Annaiah RH, Nanni A. Strengthening of short shear span reinforced concrete T joists with fiber-reinforced plasic composites. J Compos Constr 2002;6:264–71. https://doi.org/10.1061/(ASCE)1090-0268(2002)6:4(264).
[69] Ramírez ALA. Análisis de los modelos de comportamiento de vigas de hormigón armado reforzadas a cortante con polímeros armados con fibras (FRP). Validación y calibración experimental 2012.
[70] Bukhari IA, Vollum RL, Ahmad S, Sagaseta J. Shear strengthening of reinforced concrete beams with CFRP. Mag Concr Res 2010;62:65–77. https://doi.org/10.1680/macr.2008.62.1.65.
[71] Qin S, Dirar S, Yang J, Chan AHC, Elshafie M. CFRP Shear strengthening of reinforced-concrete T-beams with corroded shear links. J Compos Constr 2015;19:4014081. https://doi.org/10.1061/(ASCE)CC.1943-5614.0000548.
[72] Dirar S, Lees JM, Morley CT. Precracked reinforced concrete t-beams repaired in shear with prestressed carbon fiber-reinforced polymer straps. ACI Struct J 2013;110(855–65). https://doi.org/10.14359/51685838.
[73] El-Saikaly G, Chaallal O. Fatigue behavior of RC T-beams strengthened in shear with EB CFRP L-shaped laminates. Compos Part B Eng 2015;68:100–12. https://doi.org/10.1016/j.compositesb.2014.08.014.
[74] Tetta ZC, Koutas LN, Bournas DA. Textile-reinforced mortar (TRM) versus fiber-reinforced polymers (FRP) in shear strengthening of concrete beams. Compos Part B Eng 2015;77:338–48. https://doi.org/10.1016/j.compositesb.2015.03.055.
[75] El-Maaddawy T, Chekfeh Y. Shear strengthening of t-beams with corroded stirrups using composites. ACI Struct J 2013;110(779–89). https://doi.org/10.14359/51685831.
[76] Chen GM, Zhang Z, Li YL, Li XQ, Zhou CY. T-section RC beams shear-strengthened with anchored CFRP U-strips. Compos Struct 2016;144:57–79. https://doi.org/10.1016/j.compstruct.2016.02.033.
[77] Frederick FFR, Sharma UK, Gupta VK. Influence of end anchorage on shear strengthening of reinforced concrete beams using CFRP composites. Curr Sci 2017;112(973–81). https://doi.org/10.18520/cs/v112/i05/973-981.
[78] Mhanna HH, Hawileh RA, Abdalla JA. Shear strengthening of reinforced concrete beams using CFRP wraps. Procedia Struct Integr 2019;17:214–21. https://doi.org/10.1016/j.prostr.2019.08.029.
[79] Pellegrino C, Modena C. Fiber-reinforced polymer shear strengthening of reinforced concrete beams: experimental study and analytical modeling. ACI Struct J 2006;103(720–8). https://doi.org/10.14359/16924.
[80] Funakawa SK, Watanabe T, Asada S, e Ushijima SI. Experimental study on shear strenghthening with continuous fiber reinforcement sheet and methacrylate resin Proceeding Third Int Symp Non-Metallic(FRP)Reinforcement. Concr Strutures 1997;1:475–82.
[81] Kamiharako A, Maruyama K, Takada K, T S. Evaluation of shear contribution of FRP sheets attached to concrete beams. Proc. third Int. Symp. Non-Metallic FRP Reinf. Concr. Struct., Tokyo,Japan; 1997.
[82] Sato Y. Ultimate shear capacity of reinforced concrete beams with carbon fiber sheet. Proc. Third Int. Symp. Non-Metallic Reinf. Concr. Syructures, vol. 1, 1997, p. 499–506.
[83] Barros JA, Dias SJ. Near surface mounted CFRP laminates for shear strengthening of concrete beams. Cem Concr Compos 2006;28:276–92. https://doi.org/10.1016/j.cemconcomp.2005.11.003.
[84] Li A, Diagana C, Delmas Y. Shear strengthening effect by bonded composite fabrics on RC beams. Compos Part B Eng 2002;33:225–39. https://doi.org/10.1016/S1359-8368(02)00003-3.
[85] Dias SJE, Barros JAO. Performance of reinforced concrete T beams strengthened in shear with NSM CFRP laminates. Eng Struct 2010;32:373–84. https://doi.org/10.1016/j.engstruct.2009.10.001.
[86] Teng JG, Chen GM, Chen JF, Rosenboom OA, Lam L. Behavior of RC beams shear strengthened with bonded or unbonded FRP wraps. J Compos Constr 2009;13:394–404.
[87] Manos G, Kourtides V, Matsukas P. Investigation of the flexural and shear capacity of simple R/C beam specimens including repair schemes with fiber reinforced plastics. Proc. eighth Int. Symp. fibre-reinforced Polym. Reinf. Concr. Struct. (FRPRCS-8)University Patras, Patras, Greece, 2007.
[88] Farghal OA. Fatigue behavior of RC T-beams strengthened in shear with CFRP sheets. Ain Shams Eng J 2014;5:667–80. https://doi.org/10.1016/j.asej.2014.03.007.
[89] Paul W. Carbon fibre-reinforced polymer plates as shear strengthening for beams. Mater Struct 2003;36:291–301.
[90] EN 1992-1-1: Eurocode 2 - Design of concrete structures – Part 1-1: General rules and rules for buildings. Brussels: European committee for standardisation; 1991.
[91] Collins MP. Evaluation of shear design procedures for concrete structures. Rep Prep CSA Tech Comm Reinf Concr Des Canada 2001.
[92] Taerwe L, Khalil H, Matthys S. Behaviour of RC beams strengthened in shear by external CFRP sheets. Proc. Third Int. Symp. Non-Metallic Reinf. Concr. Struct. (FRPRCS-3), Sapporo, 1997, p. 14–6.

[93] Song FX, Fan CZ, Jie L. Experimental research on shear strengthening of reinforde concrete beams with externally bonded CFRP sheets. China: Southeast Univ NanJing; 2004.
[94] Monti G, Liotta M. Tests and design equations for FRP-strengthening in shear. Constr Build Mater 2007;21:799–809. https://doi.org/10.1016/j.conbuildmat.2006.06.023.
[95] Jayprakash J, Abdul Aziz AA, Abang Abdullah AA, Ashrabov AA. Shear resistance of reinforced concrete beams with bidirectional carbon fibre fabric strips, Fédération internationale du béton. Proceedings of the 2nd International. 2006.
[96] Diagana C, Li A, Gedalia B, Delmas Y. Shear strengthening effectiveness with CFF strips. Eng Struct 2003;25:507–16. https://doi.org/10.1016/S0141-0296(02)00208-0.